haematologica
Journal of the Ferrata Storti Foundation

Ceritinib overcomes proteasome inhibitor resistance in multiple myeloma by suppressing the protein folding response

by Andrej Besse, Marianne Kraus, Tiberiu Totu, Marija Buljan, Antonius P.A. Janssen, Mario van der Stelt, Karin Matisikova, Jana Veprkova, Lenka Sedlarikova, Tamara Jurinakova, Marietta Truger, Claudia Haferlach, Max Mendez Lopez, K. Martin Kortum, Leo Rasche, Christoph Driessen and Lenka Besse

Received: September 23, 2025.
Accepted: December 5, 2025.

Citation: Andrej Besse, Marianne Kraus, Tiberiu Totu, Marija Buljan, Antonius P.A. Janssen, Mario van der Stelt, Karin Matisikova, Jana Veprkova, Lenka Sedlarikova, Tamara Jurinakova, Marietta Truger, Claudia Haferlach, Max Mendez Lopez, K. Martin Kortum, Leo Rasche, Christoph Driessen and Lenka Besse. Ceritinib overcomes proteasome inhibitor resistance in multiple myeloma by suppressing the protein folding response.
Haematologica. 2025 Dec 11. doi: 10.3324/haematol.2025.289245 [Epub ahead of print]

Ceritinib overcomes proteasome inhibitor resistance in multiple myeloma by suppressing the protein folding response

Andrej Besse[1,2], Marianne Kraus[1], Tiberiu Totu[3,4,5], Marija Buljan[4,5], Antonius P. A. Janssen[6], Mario van der Stelt[6], Karin Matisikova[2], Jana Veprkova[2], Lenka Sedlarikova[2], Tamara Jurinakova[7], Marietta Truger[8], Claudia Haferlach[8], Max Mendez Lopez[1], K. Martin Kortum[9], Leo Rasche[9], Christoph Driessen[1], Lenka Besse[1,2,*]

[1] Laboratory of Experimental Oncology, Division Oncology and Hematology, HOCH Health Ostschweiz, Cantonal Hospital St. Gallen, St. Gallen, Switzerland

[2] Department of Biology, Faculty of Medicine, Masaryk University, Brno, Czech Republic

[3] Department of Health Sciences and Technology, Eidgenössische Technische Hochschule Zürich (ETH), Zurich, Switzerland

[4] Department Materials Meet Life, Swiss Federal Laboratories for Materials Science and Technology (Empa), St. Gallen, Switzerland

[5] Swiss Institute of Bioinformatics (SIB), Lausanne, Switzerland

[6] Department of Molecular Physiology, Leiden Institute of Chemistry, Leiden University & Oncode Institute, CC Leiden, The Netherlands

[7] Department of Pathophysiology, Faculty of Medicine, Masaryk University, Brno, Czech Republic

[8] MLL Munich Leukemia Laboratory, Munich, Germany

[9] Department of Internal Medicine II, University Hospital Würzburg, Würzburg, Germany

Running title: Ceritinib and carfilzomib in PI-resistant MM.

*Correspondence:

Lenka Besse

Lenka.besse@med.muni.cz / lenka.besse@h-och.ch

AUTHORSHIP CONTRIBUTIONS

AB designed and performed the majority of the *in vitro* and *in vivo* experiments and prepared the manuscript and figures. MK, KM, JV, LS, and MML contributed to the *in vitro* and *in vivo* experiments. TJ performed measurements on Incucyte. MT and CH performed the RNA-seq on patients from Würzburg cohort of patients. TT and MB analyzed the patient datasets. KMK and LR provided samples from RRMM patients. APAJ and MvdS conducted the analysis of the ChEMBL database. CD secured funding and provided critical review of the data. LB conceptualized the study, secured funding, and wrote the manuscript. All authors reviewed and edited the manuscript.

FUNDING

The work was supported by Wilhelm-Sander Stiftung (2021.077.1), Cantonal Hospital St. Gallen Research Committee internal grant no 20/41 and by the project National Institute for Cancer Research (Program EXCELES, ID Project No. LX22NPO5102) - Funded by the European Union – Next Generation EU.

COMPETING INTERESTS

The authors declare that they have no competing interests.

DATA SHARING

- Raw data from RNA-sequencing and genome-wide CRSIPR/Cas9 screening (DNA-sequencing) is available at the BioStudies database from European Molecular Biology Laboratory - European Bioinformatics Institute EMBL-EBI) website, https://www.ebi.ac.uk/biostudies/ under the accession: E-MTAB-15466 and E-MTAB-15465.
- All other data are available upon request to corresponding author.

ABSTRACT

Proteasome inhibitor (PI) resistance remains a major therapeutic obstacle in the treatment of multiple myeloma (MM). MM cells demonstrate pronounced dependence on insulin and insulin-like growth factor-1 signaling via their cognate receptors, IGF-1R and INSR. In this study, we identify ceritinib, a clinically approved inhibitor of anaplastic lymphoma kinase (ALK), as a drug, which can inhibit IGF-1R/INSR activity and downstream PI3K/AKT/mTORC1 signaling. Ceritinib can overcome PI-resistance in MM when used in combination with carfilzomib. This synergy was consistently observed across *in vitro* and *in vivo* models, and primary patient-derived MM cells. Mechanistically, MM cells exploit IGF-1R/INSR signaling to sustain expression of key molecular chaperones, including HSP70 and BiP, which are critical for maintaining proteostasis under conditions of high protein synthesis and turnover. Pharmacological inhibition of IGF-1R/INSR signaling by ceritinib abrogates this adaptive stress response, thereby preventing the upregulation of cytoprotective heat shock proteins upon proteasome inhibition. This disruption results in enhanced accumulation of protein aggregates, increased protein polyubiquitination, endoplasmic reticulum stress, and activation of apoptotic pathways. Collectively, our findings support the repurposing of ceritinib in combination with carfilzomib as a translationally relevant and safe strategy to circumvent PI resistance in MM, warranting further clinical investigation in the relapsed/refractory disease setting.

INTRODUCTION

Proteasome inhibitors (PIs), including bortezomib and carfilzomib, are cornerstone therapies in the treatment of multiple myeloma (MM), effectively managing the disease in various clinical settings.[1] However, treatment with PIs is not curative, and overcoming PI resistance remains a significant unmet medical need to improve patient survival.

PIs are highly effective in MM due to the disease's unique dependency on the ubiquitin-proteasome system (UPS) to maintain protein homeostasis, balancing high protein synthesis with proper degradation and recycling. To support protein homeostasis, MM cells adapt the size and function of the endoplasmic reticulum (ER) to efficiently fold proteins and prevent aggregation, relying on molecular chaperones, such as heat-shock proteins (HSP)70 and HSP90. In response to proteasome inhibition, MM cells further upregulate these chaperones, particularly HSP70, to stabilize proteins awaiting degradation and prevent their aggregation.[2,3] Accordingly, inhibition of HSP70 and HSP90 significantly sensitizes MM cells to PIs.[4-6] However, despite their clinical promise,[4-6] HSP inhibitors have not translated into clinical success, as trials to date have failed to produce FDA-approved therapies due to their limited potency and narrow therapeutic window.[7]

In addition to UPS, insulin and insulin-like growth factor-1 (IGF-1) signaling play crucial roles in MM cell survival and resistance to PIs. Both IGF-1 and insulin act as growth factors for MM, signaling through their respective receptors, IGF-1R and INSR,[8-10] which are highly homologous but mediate distinct cellular functions.[11] IGF-1R is involved in regulating genes that control cell proliferation, while INSR regulates genes related to metabolism and the glycolytic response to stimulation.[12] IGF-1R signaling has been linked to MM survival,[13] acquired resistance to bortezomib,[14] diminishing PI efficacy,[15] while INSR signaling remains less understood. Consequently, IGF-1R inhibition showed antitumor activity with a favorable *in vivo* therapeutic window.[13] Although inhibitors targeting IGF-1R and INSR have not been successful as single agents in clinical trials for MM, compounds that target other kinases, such as anaplastic lymphoma kinase (ALK), have shown off-target activity against IGF-

1R/INSR. One such ALK inhibitor, ceritinib, which is FDA-approved for ALK-positive non-small cell lung cancer (NSCLC),[16] has shown the ability to reduce IGF-1R and INSR phosphorylation in preclinical cancer models[17-19] and could potentially provide a therapeutic approach for overcoming PI resistance in MM.

Recent studies have shown that ceritinib exhibits selective cytotoxicity in MM cell lines and patients' primary cells.[20] In this study, we show that ceritinib exhibits strong synergistic anti-MM effects with carfilzomib, both *in vitro* and *in vivo.* By inhibiting IGF-1R and INSR signaling, ceritinib disrupts the downstream PI3K/AKT/mTORC pathway and reduces the levels of HSPs, leading to the accumulation of protein aggregates. This disruption impairs pro-survival HSP response induced by carfilzomib, further triggering autophagy and apoptosis. These results highlight a promising and safe off-the-shelf combination therapy with the potential to overcome PI resistance in MM.

METHODS

Cell lines

The multiple myeloma cell lines, AMO-1, L363, RPMI-8226 and ARH-77 were purchased from ATCC or DSMZ. Cell lines adapted to bortezomib (AMO-BTZ, L363-BTZ, RPMI-BTZ, ARH-BTZ) or carfilzomib (AMO-CFZ, L363-CFZ, RPMI-CFZ, ARH-CFZ) were grown in the presence of 90 nM of the respective inhibitors as previously described.[21]

Patients' samples

Samples of patients with MM and plasma cell leukemia (PCL) and peripheral blood mononuclear cells (PBMC) from healthy volunteers were obtained at Cantonal Hospital St. Gallen, Switzerland. All samples were obtained during routine diagnostic procedures after approval by an independent cantonal ethical committee (EKSG 09/057). Written informed consent was obtained in accordance with the Declaration of Helsinki guidelines. The baseline

patient characteristics are shown in **Table S1**. PCL samples were obtained from peripheral blood, whereas MM samples were purified from bone marrow aspirates, the CD138+ plasma cells were enriched by CD138+ selection using EasySep Human Whole Blood and Bone Marrow CD138 Positive Selection Kit (StemCell Technologies, Vancouver, Canada).

In vivo experiments

Age-matched (8-10 weeks old) male and female NSG (NOD.CB17-Prkdc^{scid}/NCrCrl) mice (Charles River, Germany) were used in the experiment, in accordance with the protocol approved by the Committee for Animal Experiments (Czech Republic); application no. MSMT-16038/2024-3. One week after the intrafemoral injection of AMO-BTZ cells (50.000 cells) equipped with TdTomato and Luciferin (RRID:Addgene_72486, a kind gift from Kazuhiro Oka), treatment with vehicle (captisol, twice a week *i.v.*), carfilzomib (4 mg/kg, twice a week *i.v.*), ceritinib (25 mg/kg, daily *i.p.*), or a drug combination was initiated for 2 weeks. The animals were randomly assigned into the treatment groups. Myeloma growth was monitored twice a week with luciferin (150 mg/kg, *s.c.*) (BioVision/Abcam; Waltham, MA, USA) using LagoX imaging system (Spectral Instruments Imaging, Tucson, AZ, USA) during the entire course of the experiment. Blood glucose and hemoglobin levels were determined from a drop of blood once weekly using ACCUGENCE PLUS Multi-Monitoring system (PM800).

Genome-wide CRISPR/Cas9 Screening

A genome-wide screening was performed in the AMO-1 cell line using the Human CRISPR Knockout Pooled Library (Brunello, RRID:Addgene_73179, a kind gift from David Root and John Doench), following established protocols.[22] A screen with increasing doses of ceritinib (starting from 1μM – to 2.5μM) was performed over 18 days (representing 10 doubling times) to identify genes whose loss sensitized the cells to a low concentration of ceritinib or allowed

cell survival in the presence of higher concentrations of ceritinib, decreasing viability to 50%. Screening data were analyzed using MaGeCK-VISPR software.[23] FDR values <0.01 were considered as statistically significant.

PamGene Kinase screening

A kinase screening to identify kinase inhibition following 30 min ceritinib treatment in AMO-1 cells was performed using the PamChip® microarrays (PamGene, The Netherlands). Detailed description is provided in Supplemental material.

Multiple Myeloma Research Foundation CoMMpass dataset analysis

Transcriptomics data were downloaded from the CoMMpass study, IA-18 and included 544 MM samples (www.themmrf.org). These data were generated as part of the Multiple Myeloma Research Foundation Personalized Medicine Initiatives (https://research.themmrf.org).

More information can be found in *Supplemental Material* section.

RESULTS

ALK inhibitors in combination with carfilzomib are cytotoxic to MM cells *in vitro and in vivo*

To evaluate which ALK inhibitors exert cytotoxic effects in MM cells *in vitro*, we tested a panel of FDA-approved or clinically investigated ALK inhibitors (crizotinib, ceritinib, alectinib, brigatinib, ensartinib, lorlatinib, entrectinib) in two PI-naïve MM cell lines (AMO-1 and L363) and their bortezomib-resistant counterparts (AMO-BTZ and L363-BTZ). Among these,

ceritinib, brigatinib, and entrectinib showed the greatest efficacy. In contrast, alectinib and lorlatinib showed minimal cytotoxic effects (**Figure 1A, Supplementary Table S2**).

We selected ceritinib for further studies and confirmed strong synergy of ceritinib and carfilzomib in several PI-resistance models (**Table 1, Supplementary Figures S1-S4**). To evaluate clinical relevance, we tested the combination in primary cells isolated from MM and PCL patients who had relapsed after or progressed on PI-containing therapies. The combination demonstrated a synergistic cytotoxic effect in all patient samples tested (**Figure 1B**). The mean IC_{50} of ceritinib in MM patient samples was 1.21 µM, while no cytotoxicity was observed in PBMCs from 3 healthy donors at doses up to 12.8 µM (**Figure 1C**), suggesting a favorable therapeutic window.

Finally, we tested the combination *in vivo* using NSG mice intrafemorally injected with luciferase-expressing AMO-BTZ cells, allowing real-time tumor monitoring within the bone marrow niche. Carfilzomib alone had minimal therapeutic effect, consistent with *in vitro* cross-resistance of AMO-BTZ cells to carfilzomib.[24] However, ceritinib significantly reduced tumor burden as a monotherapy, and its combination with carfilzomib markedly suppressed tumor growth, especially at later time points (**Figure 1D**). This translated into prolonged survival in treated animals (**Figure 1E**). Drugs in monotherapy and in combination were safe and did not affect significantly mice weight, glucose and hemoglobin level during the course of treatment (**Supplementary Figures S5A-C**). Collectively, these data demonstrate that the combination of ceritinib and carfilzomib effectively overcomes PI resistance in MM across *in vitro*, *ex vivo* and *in vivo* models, even in the context of bone marrow stromal support.

Ceritinib targets the IGF-1R/INSR pathway to reverse PI resistance in MM

To identify kinases that are inhibited by ALK inhibitors in MM, we interrogated the ChEMBL database for shared off-target receptor tyrosine kinases among the ALK inhibitors that were effective in MM at low concentrations (ceritinib, brigatinib, entrectinib), but not among those

that were ineffective (alectinib, lorlatinib). This analysis revealed that alectinib and lorlatinib are highly selective for ALK, whereas ceritinib, brigatinib, and entrectinib also target FLT3, INSR, and IGF-1R at low nanomolar concentrations (**Supplementary Table S3**).

To validate that ceritinib's efficacy in MM is primarily mediated via IGF-1R/INSR inhibition, we conducted a kinase profiling assay in AMO-1 cells. The results demonstrated selective inhibition of INSR and IGF-1R following treatment with ceritinib (**Figure 2A**), alongside other non-receptor tyrosine kinases physiologically involved in B-cell receptor (BTK, BLK), T-cell receptor (LCK, ZAP70) and other type of signaling (FES, SRC), while no inhibition of FLT3 was observed. To investigate the relevance of these targets in MM, we assessed their expression in MM patient samples from CoMMpass dataset. The results showed consistently high expression of INSR in the majority of patients. IGF-1R expression was present, but low in almost all patients. ALK, FLT3, BLK, LCK, ZAP70, and FES were mostly negligible or undetectable. In addition, expression of BTK and SRC was relatively high in the majority of patients (**Figure 2B**). Expression data from PI-naïve and PI-resistant MM cell lines used in this study corroborated these findings (**Supplementary Figure S6**). Additionally, data from the Cancer Dependency Map (DepMap, www.depmap.org) indicated that plasma cell myeloma exhibits increased dependency on INSR and IGF-1R (**Supplementary Figure S7, Supplementary Table S4**) for survival, in contrast to BTK and SRC, further supporting its functional relevance in MM.

We next tested whether direct inhibition of the IGF-1R/INSR pathway with two small-molecule inhibitors of IGF-1R/INSR (BMS-536924 and NVP-AEW541), could reproduce the synergy observed between ceritinib and carfilzomib in both PI-naïve (AMO-1, L363) and PI-resistant (AMO-BTZ, L363-BTZ) cells. Application of either of the small-molecule inhibitors in a combination with carfilzomib exhibited strong synergistic cytotoxicity, particularly in PI-resistant cells (**Figure 2C, D**). Notably, combining BMS-536924 or NVP-AEW541 with ceritinib did not result in additional synergy, suggesting that these agents converge on the same signaling pathway (**Supplementary Figure S8**).

In summary, these findings demonstrate that ceritinib modulates PI resistance in MM by targeting the IGF-1R/INSR axis, and that this pathway plays a critical role in mediating resistance to proteasome inhibition.

The PI3K/Akt/mTORC1 pathway is a key mediator of ceritinib-induced cytotoxicity in MM

To identify key genes and signaling pathways mediating the cytotoxic effects of ceritinib in MM, we conducted a CRISPR/Cas9 genome-wide screen in AMO-1 cells. The screen identified 17 candidate resistance genes (FDR < 0.01; $\log_2$ fold change > 1) and 2 candidate sensitivity genes (FDR < 0.01; $\log_2$ fold change < –1) (**Figure 3A; Supplementary Table S5**). Among the resistance hits, FOXO1, NPRL2, NPRL3, DDIT4, TSC2, and TSC3 (all known negative regulators of mTORC1 signaling) were prominently enriched. These genes are also recognized as co-dependent in prior large-scale screens.[25] As FOXO transcription factors and mTORC1 represent key downstream targets of the PI3K/Akt pathway, this suggests that ceritinib may exert its anti-myeloma effects through suppression of this axis.

To independently validate our screen and assess reproducibility in additional cell lines, we pharmacologically inhibited FOXO1 using the selective inhibitor AS1842856. Combination treatment with AS1842856 significantly attenuated ceritinib-induced cytotoxicity in both AMO-1 and L363 cells (**Figure 3B, C**), confirming FOXO1 as a functional mediator of ceritinib response.

We next used functional reporter assays to monitor ceritinib's effects on PI3K/Akt signaling. In the first model, U2-OS cells expressing FOXO1-Clover and a nucleolar mCherry reporter were used to visualize FOXO1 nuclear translocation, a hallmark of PI3K/Akt inhibition. Treatment with ceritinib caused rapid translocation of GFP from the cytosol to the nucleus, consistent with pathway suppression (**Figure 3D**). In the second model, we assessed mTORC1 activity in AMO-1 cells using a TOSI (Target of mTOR Signaling Indicator)

construct, where PDCD4 is tagged with mVenus. PDCD4 is rapidly degraded upon mTORC1 activation, thus its stabilization reflects mTORC1 inhibition. Following 12 hours of ceritinib exposure, PDCD4 levels were significantly elevated in AMO-1 cells (**Figure 3E**), further supporting the suppression of mTORC1 activity.

Additionally, kinome profiling in AMO-1 cells revealed that ceritinib inhibited multiple intracellular serine/threonine kinases regulated by insulin signaling, including several ribosomal S6 kinases (RSKs), as annotated in the KEGG pathway database (**Figure 3F**). Consistently, immunoblotting demonstrated reduced phosphorylation of both p70 S6 kinase and ribosomal protein S6, key downstream components of the mTORC1-driven translation machinery (**Figure 3G, Supplementary Figure S9**).

Collectively, these results indicate that ceritinib exerts its anti-MM activity primarily through suppression of the PI3K/Akt/mTORC1 pathway, leading to FOXO1 activation, inhibition of protein synthesis, and restoration of tumor suppressive signaling.

Ceritinib impairs the heat shock response and enhances ER stress induction by carfilzomib, shifting the balance toward apoptosis.

To elucidate the molecular mechanism underlying the synergy between ceritinib and carfilzomib we performed transcriptomic profiling of differently expressed genes in AMO-1 cells 8 hours after the single and combinatorial treatments (**Supplementary Table S6**). Gene Set Enrichment Analysis (GSEA) of ceritinib-induced expression changes, as well as by Gene Ontology (GO) classification based on Biological Processes (BP), revealed that ceritinib monotherapy suppressed pathways associated with DNA replication, ribonucleoprotein (RNP) complex processing, and protein folding (**Figure 4A Supplementary Figure S10A, Supplementary Table S7**). Notably, individual genes from the significantly enriched process of protein folding are HSP involved in processing of proteins in the ER, and response to unfolded/misfolded proteins (**Figure 4A, B**), as well as

proteasome-encoding genes (**Figure 4C**). This is consistent with previous findings that insulin/IGF-1 signaling induces HSP expression.[26] In parallel, GSEA followed by network analysis and Transcription Factor (TF) target analysis (based on WebGestalt) identified E2F as a central transcription regulator of the ceritinib-repressed gene set (**Supplementary Figure S10B**), with individual genes reflecting impaired cell cycle progression (**Supplementary Figure S10C**). Genes induced by ceritinib were enriched for targets of FOXO1 TF (**Supplementary Figure S10D, E**), consistent with inhibition of PI3K/Akt signaling.

Carfilzomib monotherapy, as expected, induced the expression of genes associated with protein folding (HSP proteins), ER stress and proteasome (**Figure 4A-C, Supplementary Figure S10F, Supplementary Table S6 and S7**), consistent with previous reports.[3] At the same time, it suppressed cell cycle progression and DNA replication-associated genes (**Supplementary Table S8**).

The combination of ceritinib and carfilzomib enhanced the ER stress response as evidenced by the induction of genes related to the BP: topologically incorrect proteins, ER stress and autophagy (**Figure 4B, Supplementary Figure S10G, H**). Interestingly, despite stronger induction of ER stress, the response to protein misfolding and associated proteasome assembly appeared attenuated compared to carfilzomib monotherapy (**Figure 4A, C**), suggesting that ceritinib co-treatment impairs the critical pro-survival response, typically elicited by proteasome inhibition.[3]

Consistently, genes regulated by FOXO1, robustly induced by ceritinib alone, were also found to be elevated in the combination treatment (**Supplementary Table S9, Supplementary Figure S10E**), indicating sustained Akt signaling suppression. Moreover, the combination led to a pronounced downregulation of genes involved in DNA replication and cell cycle progression (**Figure 4F, Supplementary Table S9**), with enrichment for E2F-target repression (**Supplementary Figure S10C**).

To explore the metabolic changes induced by single and combination treatments, we conducted an untargeted metabolomic analysis of metabolites following 8 hours of treatment with each drug alone and in combination (**Supplementary Table S10**). Ceritinib and the combination treatment reduced the levels of metabolites associated with glycolysis and the 'Warburg effect', consistent with INSR inhibition.[27] Consequently, the combination treatment led to reduction of pyrimidines and accumulation of purine degradation products (guanosine, guanine, hypoxanthine, and xanthine) (**Figure 4D**), suggesting a disruption in nucleotide recycling for DNA and RNA synthesis, consistent with cell cycle arrest and imbalance in nucleotide synthesis.

At the protein level, immunoblot analysis confirmed key changes in protein folding response, observed as a reduction in HSP70 and HSPA5 (GRP78, BiP) following ceritinib treatment, both as monotherapy and in combination with carfilzomib, compared to either untreated or carfilzomib-treated PI-naïve and PI-resistant cells (**Figure 4E, F, Supplementary Figure S11A, B**). The data supports the findings observed at the transcriptome level and highlights a mechanistic shift from a cytoprotective to pro-apoptotic ER stress response during combination treatment.

Ceritinib and carfilzomib co-treatment disrupts pro-survival protein folding, triggering ER stress, polyubiquitin accumulation, autophagy, and apoptosis

Next, we investigated how ceritinib and carfilzomib co-treatment affects protein homeostasis. Using activity-based probes, we first confirmed that carfilzomib inhibits proteasome β5 subunit activity and partially inhibits β2 and β1 subunits, leading to the accumulation of polyubiquitinated proteins (K48-Ub proteins) (**Figure 5A**). While ceritinib alone had no direct effect on proteasome activity, its combination with carfilzomib led to significant poly-Ub accumulation (**Figure 5A, Supplementary Figure S12**). This finding was corroborated using the Ub-G76V-GFP reporter system, where ceritinib and carfilzomib led to significantly higher

accumulation of Ub-G76V-GFP compared to carfilzomib alone, whereas ceritinib monotherapy had no significant impact (**Figure 5B**).

We next evaluated the formation of toxic intracellular protein aggregates. Carfilzomib alone did not substantially induce aggregation, likely due to a compensatory heat-shock response that stabilizes unfolded/misfolded proteins.[3] In contrast, ceritinib monotherapy triggered the formation of aggresomes, and this effect was markedly enhanced by co-treatment with carfilzomib in both PI-naïve and BTZ-resistant MM cells, suggesting a mechanism for overcoming PI resistance (**Figure 5C**).

To assess how this accumulation of misfolded and ubiquitinated proteins impacts the unfolded protein response (UPR), we used AMO-1 cells equipped with fluorescent XBP1 splicing (XBP1s) reporter. As expected, carfilzomib strongly induced XBP1s after 8 hours, consistent with increased proteotoxic stress. Ceritinib alone caused only modest XBP1s induction, but combination treatment significantly enhanced XBP1s activation (**Figure 5D**).

We further evaluated the induction of autophagy using AMO-1 cells equipped with a tandem GFP/RFP-LC3 reporter. Ceritinib, but not carfilzomib, significantly induced autophagy within 8 hours, (**Figure 5E**), consistent with mTORC1 inhibition. Notably, the ceritinib-induced autophagic flux at lower drug concentration (2μM) was further enhanced by carfilzomib, in line with transcriptomic data.

To link these observations mechanistically to mTORC1 inhibition in MM cells, we used AMO-1 cells equipped with a PDCD4-mVenus as a reporter. Although carfilzomib alone also led to PDCD4 accumulation—likely due to blocked proteasomal degradation—the combination significantly amplified this effect, indicating cooperative suppression of mTORC1-mediated PDCD4 turnover (**Figure 5F**). Subsequently, ceritinib and carfilzomib combination significantly promoted both early and late apoptosis 24 hours after treatment (**Figure 5G**). Together, these findings demonstrate that co-inhibition of the proteasome and PI3K/Akt/mTORC1 signaling in MM disrupts protein quality control by impairing chaperone-

mediated folding, enhancing polyubiquitinated protein accumulation, and triggering autophagy.

Candidate ceritinib-resistance genes are associated with poor prognosis in MM

We next evaluated the prognostic significance of genes involved in ceritinib's mechanism of action in newly diagnosed MM patients from the CoMMpass dataset. Neither IGF-1R nor INSR showed a significant prognostic impact in this cohort (**Supplementary Figure S13A, B**). However, the highest-ranking ceritinib resistance candidates from the CRISPR screening, NPRL3 and FOXO-1, were significantly associated with poorer survival outcomes. High NPRL3 expression was associated with worse progression-free survival (PFS) and overall survival (OS) and (**Figure 6A and Supplementary Figure S13C**), while low FOXO-1 expression was only linked to shorter PFS (**Figure 6B, Supplementary Figure S13D**), but not to OS, as previously described.[28]

Additionally, high expression of DDIT4, a negative regulator of mTORC1 signaling, was significantly associated with worse PFS and OS and (**Figure 6C, Supplementary Figure S13E**), while low level of PDCD4, a marker of mTORC1 activity,[29,30] was associated with worse OS (**Supplementary Figure S13F**) in CoMMpass dataset. We also compared patients from CoMMpass dataset with that from relapsed/refractory MM (RRMM) patients from Wurzburg. IGF-1R and INSR expression was significantly elevated in the RRMM cohort of patients (**Figure 6D**).

Overall, these findings provide proof-of-concept that increased PI3K/Akt/mTORC1 activity may be associated with poorer outcomes and suggest that, in these patients and those with advanced-stage MM, combining ceritinib with carfilzomib could offer a promising therapeutic approach.

DISCUSSION

Although the IGF-1/insulin shared pathway that starts with two different receptors contributes to MM pathogenesis and resistance to standard therapies, targeting this system has shown limited clinical success, largely due to its complexity.[31] Clinical trials of IGF-1R/INSR inhibitors have yielded disappointing results due to poor efficacy, underscoring the need for novel approaches and combination strategies.

Through functional kinase screening and database analysis, we identified ceritinib, an ALK inhibitor approved for ALK-positive NSCLC, as cytotoxic in MM cells. Notably, this effect is independent of ALK, which is not expressed in MM, and instead results from ceritinib's inhibition of IGF-1R and INSR, both of which are expressed in MM and further upregulated in relapsed/refractory MM. Ceritinib demonstrated selective cytotoxicity across a panel of MM cell lines and primary MM patient samples, while showing minimal activity in other hematologic malignancies.[20]

By integrating functional genome-wide screening, RNA sequencing, and *in vitro* assays, we demonstrate that ceritinib inhibits the IGF-1R/INSR axis, leading to suppression of PI3K/Akt/mTORC1 signaling—a pathway critical for supporting the high protein synthesis demands of MM cells, particularly the production of heat shock proteins like HSP70. In parallel, INSR and IGF-1R signaling drive metabolic activity and glucose uptake, fueling nucleotide biosynthesis essential for replication, transcription, and translation. While MM cell dependence on Akt/mTORC signaling is well established,[28,32,33] our data highlight a specific reliance on IGF-1R/INSR to maintain elevated HSP70 levels, aligning with previous reports of insulin-mediated regulation of heat shock proteins and factors.[34]

FOXO-1 and cell-intrinsic negative regulators of mTORC1, including NPRL2, NPRL3, and DDIT4, play a crucial role in the cytotoxicity of ceritinib in MM cells. Activated FOXO-1 inhibits mTORC1 through both Tuberous Sclerosis Complex (TSC)2-dependent and independent mechanisms.[25] DDIT4 inhibits mTORC1 activity via the TSC1/TSC2 complex, a critical regulator of mTORC1 that is triggered by growth factors, such as insulin.[35] In contrast, NPRL2 and NPRL3 form the GATOR1 complex, which is a pivotal regulator of the pathway

that signals amino acid sufficiency to mTORC1 and inhibits mTORC1 activity during intracellular amino acid starvation.[36] Given these insights, the highly active mTORC1 complex appears to be crucial for the cytotoxicity of ceritinib. It also significantly impacts the outcome of MM patients. High FOXO-1 levels are associated with a better prognosis, while elevated NPRL3 and DDIT4 levels have a negative impact on MM patient survival. Consistently, high FOXO-1 has been associated with better OS of MM patients,[28] while low FOXO-1 levels correlate with poor prognosis in patients with myelodysplastic syndrome (MDS).[37] Similarly, DDIT4 is associated with poor prognosis in solid tumors,[38,39] as well as in hematologic cancers, such as acute myeloid leukemia[40] and MM.[41]

Our data demonstrate that ceritinib can be combined with carfilzomib to overcome PI resistance in multiple MM cell lines *in vitro*, in primary samples of RRMM and PCL patients, and in an orthotopic PI-resistant *in vivo* model. This is particularly important in the context of bone marrow microenvironment-driven MM resistance, which is mediated by the interaction between MM cells and surrounding mesenchymal stem cells, and which depends on high PI3K/Akt/mTOR signaling.[42] Consistently, selective Akt inhibition enhances cytotoxicity of proteasome inhibition.[43] The strong synergy between ceritinib and carfilzomib reflects dual disruption of protein homeostasis, specifically protein folding and degradation. Carfilzomib induces a pro-survival induction of heat shock proteins and chaperons actively compensating for the inability to degrade proteins.[3] In line with this, selective inhibition of HSP70 sensitizes multiple cell lines to carfilzomib.[3] Since ceritinib inhibits HSP70 protein induction, the combination treatment results in the accumulation of protein aggregates, ER stress, and autophagy in MM cells, collectively promoting apoptosis. Additionally, mTORC1 and the UPS are tightly linked through amino acid and nutrient sensing. mTORC1 inhibition activates both the UPS and autophagy, promoting amino acid recycling and slowing cell growth,[44,45] while proteasome inhibition depletes amino acids, triggering cell death if not replenished.[46] This dependency on protein recycling has been exploited therapeutically.[47] Previous preclinical data with novel inhibitors of PI3K/Akt/mTORC1 pathway (copanlisib, montelukast) or

depletion of amino acids in combination with carfilzomib reported synergistic drug combination in PI-sensitive and PI-resistant models[48-50] supporting our findings of dual targeting of these pathways to achieve an anti-MM effect.

While these data provide compelling preclinical evidence for the combination of ceritinib and carfilzomib, certain limitations should be acknowledged. The use of proteasome inhibitor–adapted cell lines generated in vitro may not fully represent the complexity and heterogeneity of clinical resistance. Furthermore, xenograft studies based on these lines do not reproduce the full immune and stromal interactions of the human bone marrow microenvironment, underscoring the need for validation in patient-derived models.

In summary, these findings highlight a potential off-the-shelf combination therapy that could overcome therapy resistance in MM and provide a strong rationale for further preclinical and clinical testing in the RRMM setting.

REFERENCES

1. Gandolfi S, Laubach JP, Hideshima T, et al. The proteasome and proteasome inhibitors in multiple myeloma. Cancer Metastasis Rev. 2017;36(4):561-584.

2. Mitsiades N, Mitsiades CS, Poulaki V, et al. Molecular sequelae of proteasome inhibition in human multiple myeloma cells. Proc Natl Acad Sci U S A. 2002;99(22):14374-14379.

3. Oron M, Grochowski M, Jaiswar A, et al. The molecular network of the proteasome machinery inhibition response is orchestrated by HSP70, revealing vulnerabilities in cancer cells. Cell Rep. 2022;40(13):111428.

4. Huang L, Wang Y, Bai J, et al. Blockade of HSP70 by VER-155008 synergistically enhances bortezomib-induced cytotoxicity in multiple myeloma. Cell Stress Chaperones. 2020;25(2):357-367.

5. Ishii T, Seike T, Nakashima T, et al. Anti-tumor activity against multiple myeloma by combination of KW-2478, an Hsp90 inhibitor, with bortezomib. Blood Cancer J. 2012;2(4):e68.

6. Ferguson ID, Lin YT, Lam C, et al. Allosteric HSP70 inhibitors perturb mitochondrial proteostasis and overcome proteasome inhibitor resistance in multiple myeloma. Cell Chem Biol. 2022;29(8):1288-1302.

7. Seggewiss-Bernhardt R, Bargou RC, Goh YT, et al. Phase 1/1B trial of the heat shock protein 90 inhibitor NVP-AUY922 as monotherapy or in combination with bortezomib in patients with relapsed or refractory multiple myeloma. Cancer. 2015;121(13):2185-2192.

8. Georgii-Hemming P, Wiklund HJ, Ljunggren O, Nilsson K. Insulin-like growth factor I is a growth and survival factor in human multiple myeloma cell lines. Blood. 1996;88(6):2250-2258.

9. Sprynski AC, Hose D, Caillot L, et al. The role of IGF-1 as a major growth factor for myeloma cell lines and the prognostic relevance of the expression of its receptor. Blood. 2009;113(19):4614-4626.

10. Sprynski AC, Hose D, Kassambara A, et al. Insulin is a potent myeloma cell growth factor through insulin/IGF-1 hybrid receptor activation. Leukemia. 2010;24(11):1940-1950.

11. De Meyts P, Whittaker J. Structural biology of insulin and IGF1 receptors: implications for drug design. Nat Rev Drug Discov. 2002;1(10):769-783.

12. Cai W, Sakaguchi M, Kleinridders A, et al. Domain-dependent effects of insulin and IGF-1 receptors on signalling and gene expression. Nat Commun. 2017;8:14892.

13. Mitsiades CS, Mitsiades NS, McMullan CJ, et al. Inhibition of the insulin-like growth factor receptor-1 tyrosine kinase activity as a therapeutic strategy for multiple myeloma, other hematologic malignancies, and solid tumors. Cancer Cell. 2004;5(3):221-230.

14. Kuhn DJ, Berkova Z, Jones RJ, et al. Targeting the insulin-like growth factor-1 receptor to overcome bortezomib resistance in preclinical models of multiple myeloma. Blood. 2012;120(16):3260-3270.

15. Tanaka Y, Okabe S, Tauchi T, Ito Y, Ohyashiki K. Targeting Insulin-like Growth Factor in Multiple Myeloma: Novel Strategies in the Treatment of Proteasome Inhibitor Resistant Cells. Blood. 2018;132(Supplememnt 1):5155.

16. Shaw AT, Kim DW, Mehra R, et al. Ceritinib in ALK-rearranged non-small-cell lung cancer. N Engl J Med. 2014;370(13):1189-1197.

17. van Erp AEM, Hillebrandt-Roeffen MHS, van Houdt L, Fleuren EDG, van der Graaf WTA, Versleijen-Jonkers YMH. Targeting Anaplastic Lymphoma Kinase (ALK) in Rhabdomyosarcoma (RMS) with the Second-Generation ALK Inhibitor Ceritinib. Target Oncol. 2017;12(6):815-826.

18. Vewinger N, Huprich S, Seidmann L, et al. IGF1R Is a Potential New Therapeutic Target for HGNET-BCOR Brain Tumor Patients. Int J Mol Sci. 2019;20(12):3027.

19. Russo A, Paret C, Alt F, et al. Ceritinib-Induced Regression of an Insulin-Like Growth Factor-Driven Neuroepithelial Brain Tumor. Int J Mol Sci. 2019;20(17):4267.

20. Bonolo de Campos C, Meurice N, Petit JL, et al. "Direct to Drug" screening as a precision medicine tool in multiple myeloma. Blood Cancer J. 2020;10(5):54.

21. Besse A, Besse L, Kraus M, et al. Proteasome Inhibition in Multiple Myeloma: Head-to-Head Comparison of Currently Available Proteasome Inhibitors. Cell Chem Biol. 2019;26(3):340-351.

22. Besse L, Besse A, Stolze SC, et al. Treatment with HIV-Protease Inhibitor Nelfinavir Identifies Membrane Lipid Composition and Fluidity as a Therapeutic Target in Advanced Multiple Myeloma. Cancer Res. 2021;81(17):4581-4593.

23. Li W, Koster J, Xu H, et al. Quality control, modeling, and visualization of CRISPR screens with MAGeCK-VISPR. Genome Biol. 2015;16:281.

24. Soriano GP, Besse L, Li N, et al. Proteasome inhibitor-adapted myeloma cells are largely independent from proteasome activity and show complex proteomic changes, in particular in redox and energy metabolism. Leukemia. 2016;30(11):2198-2207.

25. Chen CC, Jeon SM, Bhaskar PT, et al. FoxOs inhibit mTORC1 and activate Akt by inducing the expression of Sestrin3 and Rictor. Dev Cell. 2010;18(4):592-604.

26. Geffken SJ, Moon S, Smith CO, et al. Insulin and IGF-1 elicit robust transcriptional regulation to modulate autophagy in astrocytes. Mol Metab. 2022;66:101647.

27. Yee LD, Mortimer JE, Natarajan R, Dietze EC, Seewaldt VL. Metabolic Health, Insulin, and Breast Cancer: Why Oncologists Should Care About Insulin. Front Endocrinol (Lausanne). 2020;11:58.

28. Bloedjes TA, de Wilde G, Maas C, et al. AKT signaling restrains tumor suppressive functions of FOXO transcription factors and GSK3 kinase in multiple myeloma. Blood Adv. 2020;4(17):4151-4164.

29. Moustafa-Kamal M, Kucharski TJ, El-Assaad W, et al. The mTORC1/S6K/PDCD4/eIF4A Axis Determines Outcome of Mitotic Arrest. Cell Rep. 2020;33(1):108230.

30. Paroha R, Wang J, Lee S. PDCD4 as a marker of mTOR pathway activation and therapeutic target in mycobacterial infections. Microbiol Spectr. 2024;12(8):e0006224.

31. Bieghs L, Johnsen HE, Maes K, et al. The insulin-like growth factor system in multiple myeloma: diagnostic and therapeutic potential. Oncotarget. 2016;7(30):48732-48752.

32. Hsu J, Shi Y, Krajewski S, et al. The AKT kinase is activated in multiple myeloma tumor cells. Blood. 2001;98(9):2853-2855.

33. Peterson TR, Laplante M, Thoreen CC, et al. DEPTOR is an mTOR inhibitor frequently overexpressed in multiple myeloma cells and required for their survival. Cell. 2009;137(5):873-886.

34. Ting LP, Tu CL, Chou CK. Insulin-induced expression of human heat-shock protein gene hsp70. J Biol Chem. 1989;264(6):3404-3408.

35. Tirado-Hurtado I, Fajardo W, Pinto JA. DNA Damage Inducible Transcript 4 Gene: The Switch of the Metabolism as Potential Target in Cancer. Front Oncol. 2018;8:106.

36. Bar-Peled L, Chantranupong L, Cherniack AD, et al. A Tumor suppressor complex with GAP activity for the Rag GTPases that signal amino acid sufficiency to mTORC1. Science. 2013;340(6136):1100-1106.

37. Zhang Z, Huang N, Xv F, et al. Decreased FOXO1 Expression Is Correlated with Poor Prognosis in Myelodysplastic Syndromes. Curr Oncol. 2022;29(10):6933-6946.

38. Song L, Chen Z, Zhang M, et al. DDIT4 overexpression associates with poor prognosis in lung adenocarcinoma. J Cancer. 2021;12(21):6422-6428.

39. Chen X, Li Z, Liang M et, al. Identification of DDIT4 as a potential prognostic marker associated with chemotherapeutic and immunotherapeutic response in triple-negative breast cancer. World J Surg Oncol. 2023;21(1):194.

40. Cheng Z, Dai Y, Pang Y, et al. Up-regulation of DDIT4 predicts poor prognosis in acute myeloid leukaemia. J Cell Mol Med. 2020;24(1):1067-1075.

41. Yu Z, Qiu B, Li L, Xu J, Zhou H, Niu T. An emerging prognosis prediction model for multiple myeloma: Hypoxia-immune related microenvironmental gene signature. Front Oncol. 2022;12:992387.

42. Heinemann L, Mollers KM, Ahmed HMM, et al. Inhibiting PI3K-AKT-mTOR Signaling in Multiple Myeloma-Associated Mesenchymal Stem Cells Impedes the Proliferation of Multiple Myeloma Cells. Front Oncol. 2022;12:874325.

43. Mimura N, Hideshima T, Shimomura T, et al. Selective and potent Akt inhibition triggers anti-myeloma activities and enhances fatal endoplasmic reticulum stress induced by proteasome inhibition. Cancer Res. 2014;74(16):4458-4469.

44. Zhao J, Zhai B, Gygi SP, Goldberg AL. mTOR inhibition activates overall protein degradation by the ubiquitin proteasome system as well as by autophagy. Proc Natl Acad Sci U S A. 2015;112(52):15790-15797.

45. Zhao J, Garcia GA, Goldberg AL. Control of proteasomal proteolysis by mTOR. Nature. 2016;529(7586):E1-2.

46. Suraweera A, Munch C, Hanssum A, Bertolotti A. Failure of amino acid homeostasis causes cell death following proteasome inhibition. Mol Cell. 2012;48(2):242-253.

47. Saavedra-Garcia P, Roman-Trufero M, Al-Sadah HA, et al. Systems level profiling of chemotherapy-induced stress resolution in cancer cells reveals druggable trade-offs. Proc Natl Acad Sci U S A. 2021;118(17):e2018229118

48. Okabe S, Tanaka Y, Tauchi T, Ohyashiki K. Copanlisib, a novel phosphoinositide 3-kinase inhibitor, combined with carfilzomib inhibits multiple myeloma cell proliferation. Ann Hematol. 2019;98(3):723-733.

49. Tong J, Yu Q, Xu W, et al. Montelukast enhances cytocidal effects of carfilzomib in multiple myeloma by inhibiting mTOR pathway. Cancer Biol Ther. 2019;20(3):381-390.

50. Soncini D, Minetto P, Martinuzzi C, et al. Amino acid depletion triggered by L-asparaginase sensitizes MM cells to carfilzomib by inducing mitochondria ROS-mediated cell death. Blood Adv. 2020;4(18):4312-4326.

Table 1: Coefficients of drug interaction (CDI) for ceritinib in combination with either bortezomib or carfilzomib, as determined from viability assays (Supplementary Tables S1–S4) in a panel of proteasome inhibitor–naïve, bortezomib-adapted, and carfilzomib-adapted cell lines.

Cell line	**Ceritinib combination (CDI)**	
	Bortezomib	Carfilzomib
AMO-1	0.96	**0.14**
AMO-BTZ	0.79	**0.18**
AMO-CFZ	**0.24**	**0.07**
L363	0.86	0.55
L363-BTZ	0.6	**0.43**
L363-CFZ	**0.07**	**0.23**
ARH-77	0.97	**0.77**
ARH-BTZ	0.55	**0.16**
ARH-CFZ	**0.07**	**0.08**
RPMI-8226	0.97	**0.13**
RPMI-BTZ	0.52	**0.32**
RPMI-CFZ	**0.39**	**0.2**

FIGURE LEGENDS

Figure 1: The combination of ceritinib and carfilzomib exhibits strong synergistic activity both *in vitro* and *in vivo*.

(A) Dose–response curves of seven clinically available ALK inhibitors in PI-naïve MM cell lines (L363 and AMO-1) and their bortezomib-adapted counterparts (L363-BTZ and AMO-BTZ). The data represent the mean ± SD from at least three independent biological replicates.

(B) Cytotoxicity of the ceritinib and carfilzomib combination in primary samples from MM patients (red scale) and plasma cell leukemia (PCL) patients (blue scale). A CDI was calculated for each patient. The data represent the mean ± SD from technical quadruplicates.

(C) IC_{50} values of ceritinib in primary samples from MM and PCL patients, as well as in PBMCs from healthy donors (HD). The data represent ranges from three individual samples per cohort.

(D) *In vivo* imaging of luminescence intensity from orthotopically implanted AMO-BTZ cells, shown as fold change normalized to Day 7 (treatment initiation). The number of animals per group (*n*) is indicated in the treatment conditions. The data represent the mean ± SD for each treatment cohort. Statistical significance was assessed by two-way ANOVA with Tukey's post hoc test: ****$p < 0.0001$, ***$p < 0.001$, **$p < 0.01$, *$p < 0.05$.

(E) Kaplan-Meier curves illustrating survival of mice with orthotopically implanted AMO-BTZ cells and treated with respective drugs and combination. The number of animals per group (*n*) is indicated in the treatment conditions. Statistical analysis was performed using log-rank (Mantel-Cox) test.

CDI = coefficient of drug interaction; ceri = ceritinib; CFZ = carfilzomib; HD = healthy donor; MM = multiple myeloma; PBMC = peripheral blood mononuclear cells; PCL = plasma cell leukemia; PI = proteasome inhibitor; SD = standard deviation

Figure 2. Ceritinib enhances carfilzomib efficacy by targeting highly expressed INSR/IGF-1R in multiple myeloma.

(A) Volcano plot depicting the kinase inhibition profile in AMO-1 cells 30 minutes after treatment with 4 μM ceritinib. IGF-1R and INSR are highlighted in red.

(B) Violin plot illustrating the expression of the off-target kinases identified by ceritinib in a cohort of 590 newly diagnosed MM patients, based on the MMRF CoMMpass dataset. The data represent normalized transcript counts.

(C) Cytotoxic effects of CFZ and the IGF-1R/INSR small molecule inhibitor NVP-AEW541 in PI-naïve (AMO-1, L363) and PI-adapted (AMO-BTZ, AMO-CFZ) cell lines. The data represent the mean ± SD from three independent biological replicates. CDIs for combination treatment are presented.

(D) Cytotoxic effects of CFZ and the IGF-1R/INSR inhibitor BMS-536924 in PI-naïve (AMO-1, L363) and PI-adapted (AMO-BTZ, AMO-CFZ) cell lines. The data represent the mean ± SD from three independent biological replicates. CDIs for combination treatment are presented.

CDI = coefficient of drug interaction; CFZ = carfilzomib; INSR = insulin receptor; IGF-1R = insulin-like growth factor 1 receptor; PI = proteasome inhibitor; SD = standard deviation

Figure 3. Ceritinib inhibits downstream PI3K/Akt/mTORC1 signaling in MM cells via inhibition of IGF-1R/INSR.

(A) Volcano plot showing sensitivity (blue) and resistance (red) genes to ceritinib, identified through a genome-wide CRISPR/Cas9 screen performed in AMO-1 cells.

(B–C) Validation of CRISPR screen hits using the FOXO1 small-molecule inhibitor AS1842856 in (B) AMO-1 and (C) L363 MM cell lines, either as monotherapy or in combination with ceritinib. The data represent the mean ± SD from three independent biological replicates. Statistical significance was determined using two-way ANOVA with Tukey's post hoc test; *$p < 0.05$.

(D) Quantification of FOXO1-clover nucleolar translocation in the U2-OS model cell line expressing a nucleolar mCherry reporter. The fraction of cytosolic GFP-only signal was measured at 2, 4, and 6 hours following treatment with the indicated doses of ceritinib. The data represent the mean ± SD from four replicates. Statistical significance was assessed by two-way ANOVA with Tukey's post hoc test; ****$p < 0.0001$.

(E) Quantification of PDCD4-mVenus fluorescence intensity in AMO-1 cells 12 hours after treatment with 4 µM ceritinib. The data represent the mean ± SD from three independent experiments, each performed in triplicate. Statistical significance was determined by unpaired t-test; ****$p < 0.0001$.

(F) STK inhibited by ceritinib in AMO-1 cells following an 8-hour treatment with 4 µM ceritinib, ranked by median kinase score as calculated by PamGene analysis and grouped according to insulin-related processes defined by KEGG pathway annotations.

(G) Western blot image showing phosphorylation levels of ribosomal p70 S6 kinase and ribosomal S6 protein after treatment with 4 µM ceritinib.

FOXO1 = Forkhead Box O1; GFP = green fluorescence protein; KEGG = Kyoto Encyclopedia of Genes and Genomes; MM = multiple myeloma; PDCD4 = Programmed Cell Death 4; SD = standard deviation; STK = serine threonine kinases

Figure 4. Ceritinib diminishes the endoplasmic reticulum stress and protein folding response, a key pro-survival pathway following proteasome inhibition

(A) Heatmap of leading-edge genes deregulated in AMO-1 cells 8 hours after treatment with ceritinib, carfilzomib, or their combination, clustered according to the Protein folding GO BP term. Depicted are genes with Log2FC > 0.8 (adj. $p < 0.05$) for CFZ and Log2FC < 0.8 for Ceritinib

(B) Heatmap of leading-edge genes upregulated in AMO-1 cells 8 hours after treatment with ceritinib, carfilzomib, or their combination, clustered according to the Response to

endoplasmic reticulum stress GO BP term. Depicted are genes with Log2FC > 0.8 for CFZ + Ceritinib treatment (adj. $p < 0.05$)

(C) Heatmap of leading-edge genes upregulated in AMO-1 cells 8 hours after treatment with 4 μM ceritinib, 5 nM carfilzomib, and their combination, clustered according to the Proteasome GO BP term. The data were normalized to untreated control samples and represent Log2 FC values.

(D) Heatmap of significantly deregulated metabolites involved in glucose (Warburg effect) and purine/pyrimidine metabolism following 8-hour treatment with 4μM ceritinib, 5nM carfilzomib and their combination. The data were normalized to untreated control samples at the same time point and represent Log2 FC values at adj. $p < 0.05$.

(E) Western blot analysis showing levels of heat shock proteins HSP70 and HSPA5 (GRP78, BiP) at 4- and 8-hours following treatment with 4 μM ceritinib, 5 nM carfilzomib, or their combination (C+C) in AMO-1 cells.

(F) Western blot analysis showing levels of heat shock proteins HSP70 and HSPA5 (GRP78, BiP) in L363, AMO-BTZ and L363-BTZ cell lines 8-hours following treatment with 5 nM carfilzomib, or combination of carfilzomib with 4μM ceritinib (C+C).

BP = Biological Process; ER= Endoplasmic reticulum; GO = Gene Ontology

Figure 5. Ceritinib and carfilzomib synergistically induce polyubiquitinated protein accumulation, protein aggregation, and PDCD4 stabilization, triggering the unfolded protein response and autophagy, leading to terminal apoptosis.

(A) Representative gel and Western blot analysis showing the activity of proteasome β1c/i, β2c/i, and β5c/i subunits, along with levels of polyubiquitinated proteins, following 8-hour treatment with 5 nM carfilzomib, 4 μM ceritinib, or their combination. α-tubulin was used as a loading control.

(B) MFI of Ub-G76V-GFP reporter in AMO-1 cells after 12-hour treatment with the indicated drugs. The data represent the mean ± SD from six independent experiments. Statistical significance was assessed by one-way ANOVA; *p < 0.05, ****p < 0.0001.

(C) MFI of PROTEOSTAT® fluorescence, indicating protein aggregation in AMO-1 and PI-adapted AMO-BTZ cells, after 20-hour treatment with 5 nM carfilzomib, 4 µM ceritinib, or their combination. The data represent the mean ± SD from at least five independent experiments. Statistical analysis was assessed by one-way ANOVA; *p < 0.05, **p < 0.01, ***p < 0.001.

(D) MFI of spliced XBP1 in AMO-1 cells after 8-hour treatment. The data represent the mean ± SD from three independent experiments. Statistical significance was determined by one-way ANOVA; ***p < 0.001.

(E) Ratio of RFP (pH-unstable) to GFP (pH-stable) fluorescence in endosomal pH sensor assay in AMO-1 cells treated for 8 hours with the indicated drugs. The data represent the mean ± SD from three independent experiments. Statistical significance was assessed by one-way ANOVA: *p < 0.05, **p < 0.01, ***p < 0.001.

(F) MFI of PDCD4-mVenus reporter in AMO-1 cells after 12-hour treatment. The data represent the mean ± SD from three independent experiments in duplicate. Statistical significance was assessed by one-way ANOVA: ****p < 0.0001.

(G) Quantification of early (Annexin $V^+/FITC^-$) and late (Annexin $V^+/FITC^+$) apoptotic cells in AMO-1 after 24-hour treatment. The data represent the mean ± SD from three independent experiments. Statistical significance was assessed by two-way ANOVA; ***p < 0.001.

FITC = Fluorescein isothiocyanate; GFP = green fluorescence protein; MFI = median fluorescence intensity; RFP = red fluorescence protein; SD = standard deviation; XBP1 = X-Box Binding Protein 1;

Figure 6. Prognostic relevance of selected genes and receptor expression in MM patients.

(A) Impact of NPRL3 expression on PFS in MM patients from the CoMMpass dataset. P value was considered statistically significant at the level $p < 0.05$, statistical significance was assessed by Tarone-Ware test.

(B) Impact of FOXO1 expression on PFS in MM patients from the CoMMpass dataset. P value was considered statistically significant at the level $p < 0.05$, statistical significance was assessed by Tarone-Ware test.

(C) Impact of DDIT4 expression on PFS in MM patients from the CoMMpass dataset. P value was considered statistically significant at the level $p < 0.05$, statistical significance was assessed by Tarone-Ware test.

(D) Expression levels of IGF-1R and INSR in newly diagnosed (ND) MM patients (CoMMpass dataset) and in a cohort of RRMM patients from Würzburg University Hospital.

DDIT4 = DNA Damage Inducible Transcript 4; FOXO1 = Forkhead Box O1; IGF1R: Insulin Like Growth Factor 1 Receptor; INSR: Insulin Receptor; NPRL3 = NPR3 Like, GATOR1 Complex Subunit; PFS = progression-free survival

Figure 1

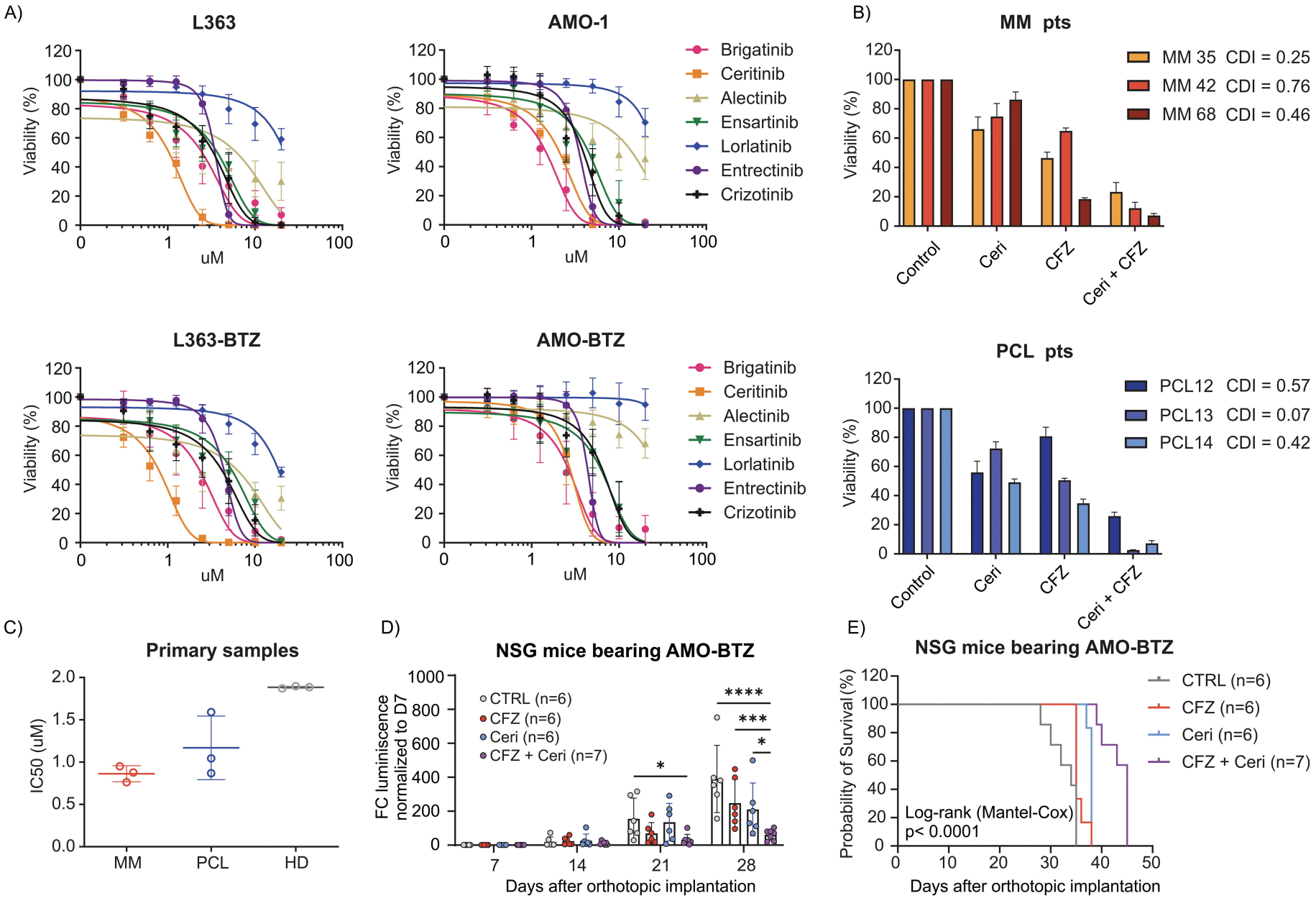
A)
L363
AMO-1
L363-BTZ
AMO-BTZ
Viability (%)
uM
Brigatinib
Ceritinib
Alectinib
Ensartinib
Lorlatinib
Entrectinib
Crizotinib
B)
MM pts
MM 35 CDI = 0.25
MM 42 CDI = 0.76
MM 68 CDI = 0.46
PCL pts
PCL12 CDI = 0.57
PCL13 CDI = 0.07
PCL14 CDI = 0.42
Control
Ceri
CFZ
Ceri + CFZ
C)
Primary samples
IC50 (uM)
MM
PCL
HD
D)
NSG mice bearing AMO-BTZ
FC luminiscence normalized to D7
CTRL (n=6)
CFZ (n=6)
Ceri (n=6)
CFZ + Ceri (n=7)
Days after orthotopic implantation
E)
NSG mice bearing AMO-BTZ
Probability of Survival (%)
Log-rank (Mantel-Cox)
p< 0.0001
Days after orthotopic implantation

Figure 2

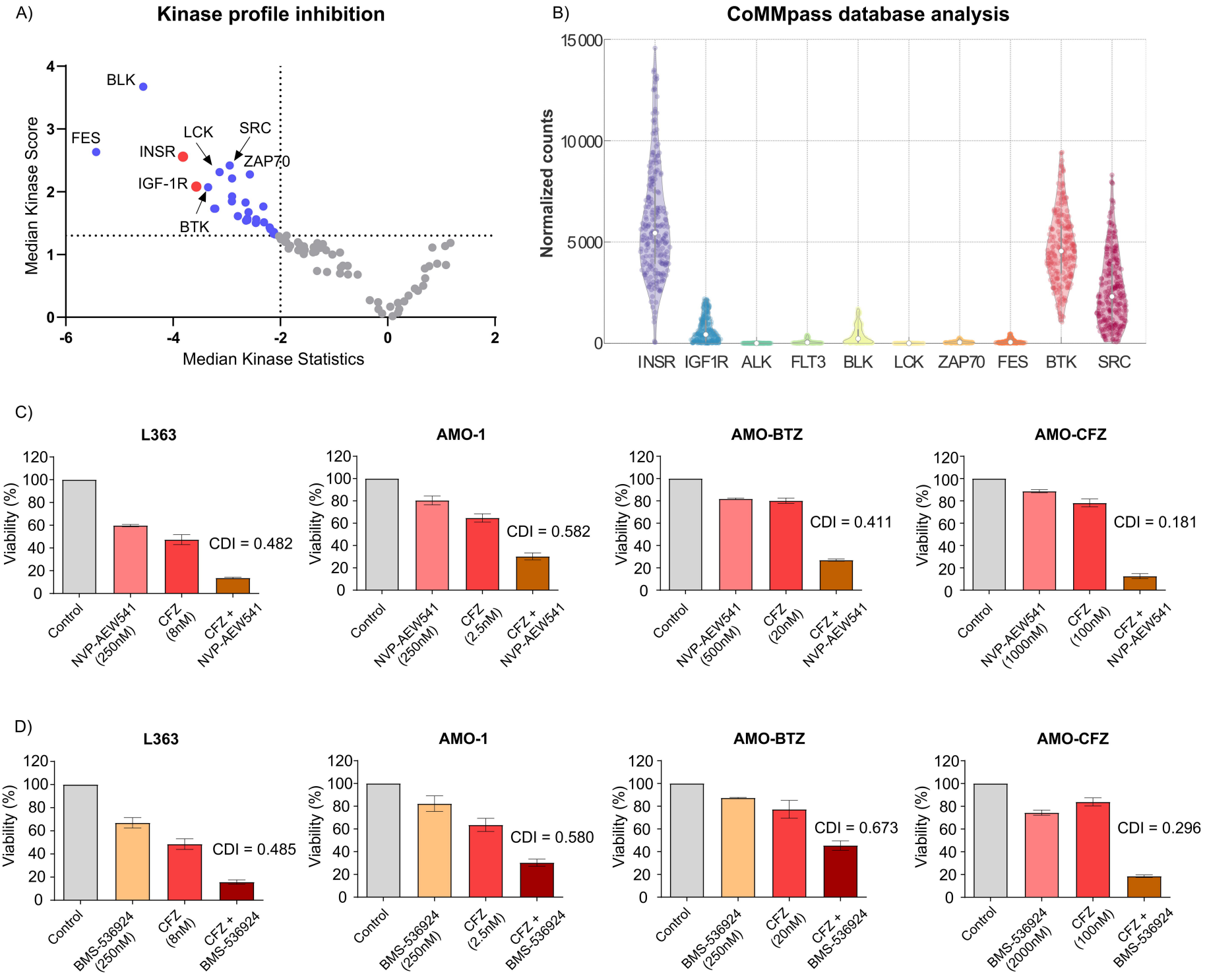
A)
Kinase profile inhibition
Median Kinase Score
Median Kinase Statistics
BLK
FES
LCK
SRC
INSR
ZAP70
IGF-1R
BTK
B)
CoMMpass database analysis
Normalized counts
INSR
IGF1R
ALK
FLT3
BLK
LCK
ZAP70
FES
BTK
SRC
C)
L363
AMO-1
AMO-BTZ
AMO-CFZ
Viability (%)
CDI = 0.482
CDI = 0.582
CDI = 0.411
CDI = 0.181
Control
NVP-AEW541 (250nM)
CFZ (8nM)
CFZ + NVP-AEW541
CFZ (2.5nM)
NVP-AEW541 (500nM)
CFZ (20nM)
NVP-AEW541 (1000nM)
CFZ (100nM)
D)
CDI = 0.485
CDI = 0.580
CDI = 0.673
CDI = 0.296
BMS-536924 (250nM)
CFZ + BMS-536924
BMS-536924 (2000nM)

Figure 3

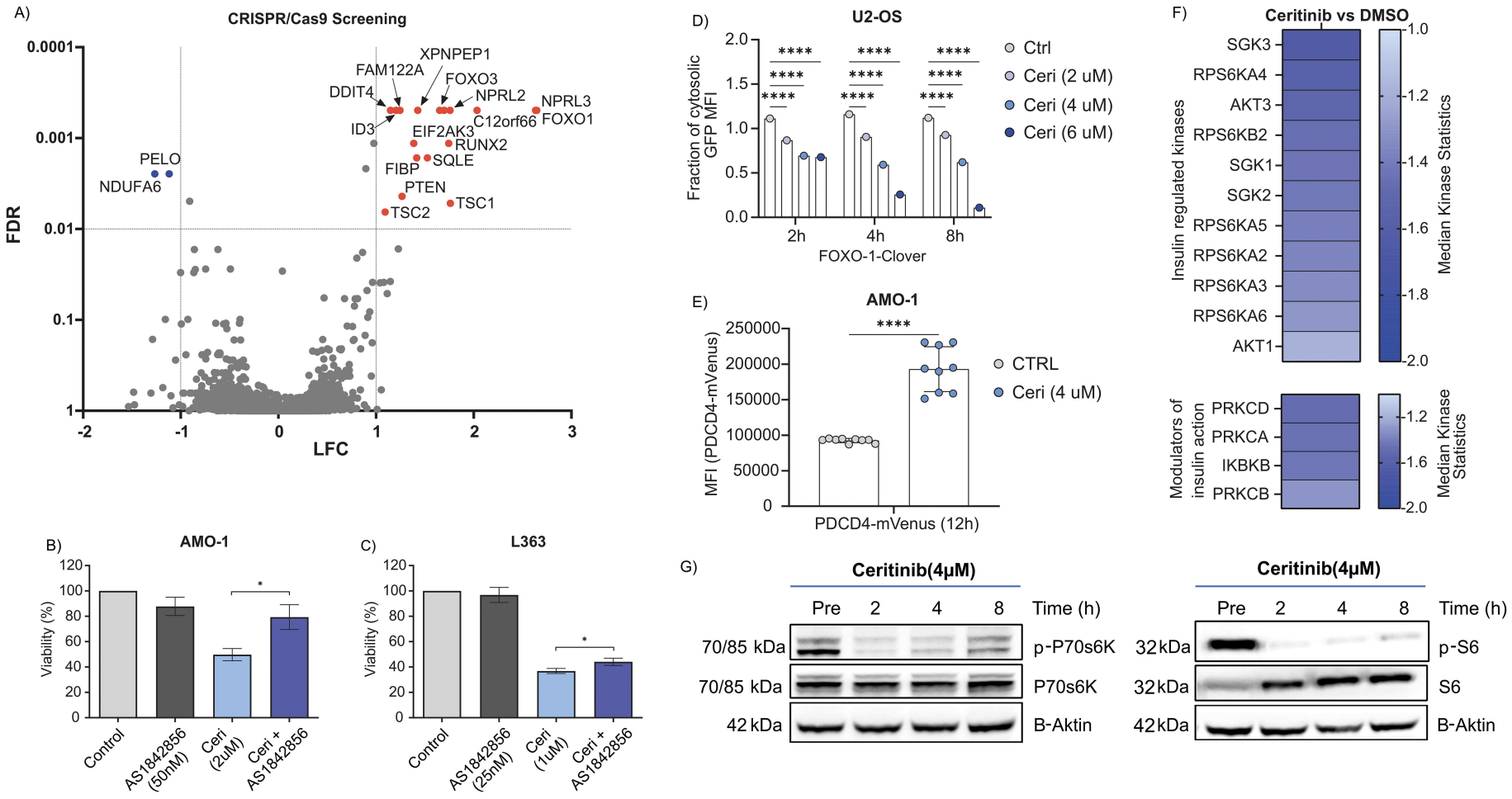
A)
CRISPR/Cas9 Screening
FDR
LFC
XPNPEP1
FAM122A
FOXO3
DDIT4
NPRL2
NPRL3
C12orf66
FOXO1
ID3
EIF2AK3
RUNX2
SQLE
FIBP
PTEN
TSC1
TSC2
PELO
NDUFA6
B)
AMO-1
Viability (%)
Control
AS1842856 (50nM)
Ceri (2uM)
Ceri + AS1842856
C)
L363
Viability (%)
Control
AS1842856 (25nM)
Ceri (1uM)
Ceri + AS1842856
D)
U2-OS
Fraction of cytosolic GFP MFI
FOXO-1-Clover
Ctrl
Ceri (2 uM)
Ceri (4 uM)
Ceri (6 uM)
E)
AMO-1
MFI (PDCD4-mVenus)
PDCD4-mVenus (12h)
CTRL
Ceri (4 uM)
F)
Ceritinib vs DMSO
Insulin regulated kinases
SGK3
RPS6KA4
AKT3
RPS6KB2
SGK1
SGK2
RPS6KA5
RPS6KA2
RPS6KA3
RPS6KA6
AKT1
Median Kinase Statistics
Modulators of insulin action
PRKCD
PRKCA
IKBKB
PRKCB
Median Kinase Statistics
G)
Ceritinib(4μM)
Pre
2
4
8
Time (h)
70/85 kDa
p-P70s6K
70/85 kDa
P70s6K
42 kDa
B-Aktin
Ceritinib(4μM)
Pre
2
4
8
Time (h)
32kDa
p-S6
32kDa
S6
42kDa
B-Aktin

Figure 4

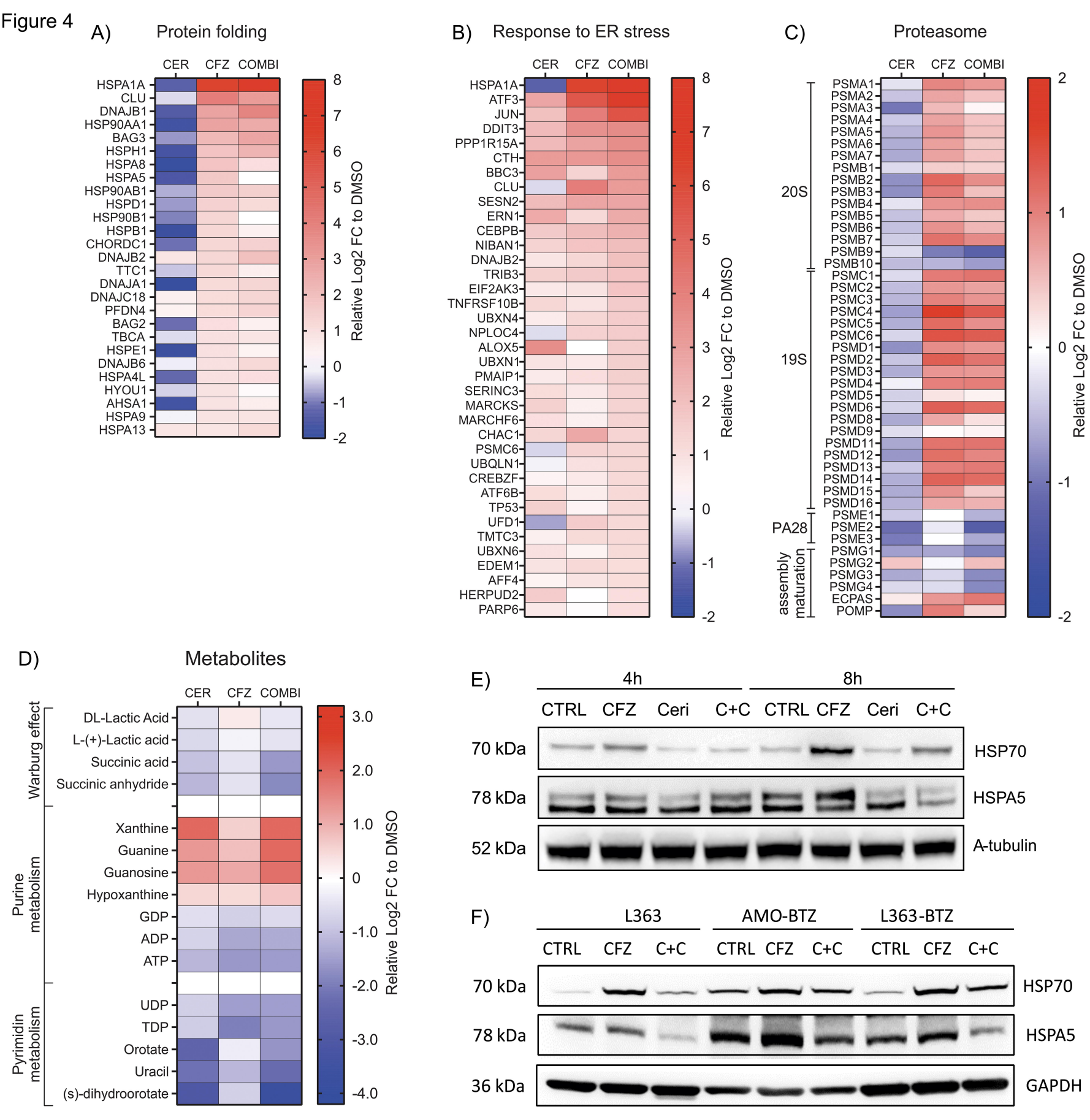
A)
Protein folding
CER
CFZ
COMBI
HSPA1A
CLU
DNAJB1
HSP90AA1
BAG3
HSPH1
HSPA8
HSPA5
HSP90AB1
HSPD1
HSP90B1
HSPB1
CHORDC1
DNAJB2
TTC1
DNAJA1
DNAJC18
PFDN4
BAG2
TBCA
HSPE1
DNAJB6
HSPA4L
HYOU1
AHSA1
HSPA9
HSPA13
8
7
6
5
4
3
2
1
0
-1
-2
Relative Log2 FC to DMSO
B)
Response to ER stress
CER
CFZ
COMBI
HSPA1A
ATF3
JUN
DDIT3
PPP1R15A
CTH
BBC3
CLU
SESN2
ERN1
CEBPB
NIBAN1
DNAJB2
TRIB3
EIF2AK3
TNFRSF10B
UBXN4
NPLOC4
ALOX5
UBXN1
PMAIP1
SERINC3
MARCKS
MARCHF6
CHAC1
PSMC6
UBQLN1
CREBZF
ATF6B
TP53
UFD1
TMTC3
UBXN6
EDEM1
AFF4
HERPUD2
PARP6
8
7
6
5
4
3
2
1
0
-1
-2
Relative Log2 FC to DMSO
C)
Proteasome
CER
CFZ
COMBI
20S
19S
PA28
assembly
maturation
PSMA1
PSMA2
PSMA3
PSMA4
PSMA5
PSMA6
PSMA7
PSMB1
PSMB2
PSMB3
PSMB4
PSMB5
PSMB6
PSMB7
PSMB9
PSMB10
PSMC1
PSMC2
PSMC3
PSMC4
PSMC5
PSMC6
PSMD1
PSMD2
PSMD3
PSMD4
PSMD5
PSMD6
PSMD8
PSMD9
PSMD11
PSMD12
PSMD13
PSMD14
PSMD15
PSMD16
PSME1
PSME2
PSME3
PSMG1
PSMG2
PSMG3
PSMG4
ECPAS
POMP
2
1
0
-1
-2
Relative Log2 FC to DMSO
D)
Metabolites
CER
CFZ
COMBI
Warburg effect
Purine metabolism
Pyrimidin metabolism
DL-Lactic Acid
L-(+)-Lactic acid
Succinic acid
Succinic anhydride
Xanthine
Guanine
Guanosine
Hypoxanthine
GDP
ADP
ATP
UDP
TDP
Orotate
Uracil
(s)-dihydroorotate
3.0
2.0
1.0
0
-1.0
-2.0
-3.0
-4.0
Relative Log2 FC to DMSO
E)
4h
8h
CTRL
CFZ
Ceri
C+C
CTRL
CFZ
Ceri
C+C
70 kDa
HSP70
78 kDa
HSPA5
52 kDa
A-tubulin
F)
L363
AMO-BTZ
L363-BTZ
CTRL
CFZ
C+C
CTRL
CFZ
C+C
CTRL
CFZ
C+C
70 kDa
HSP70
78 kDa
HSPA5
36 kDa
GAPDH

Figure 5

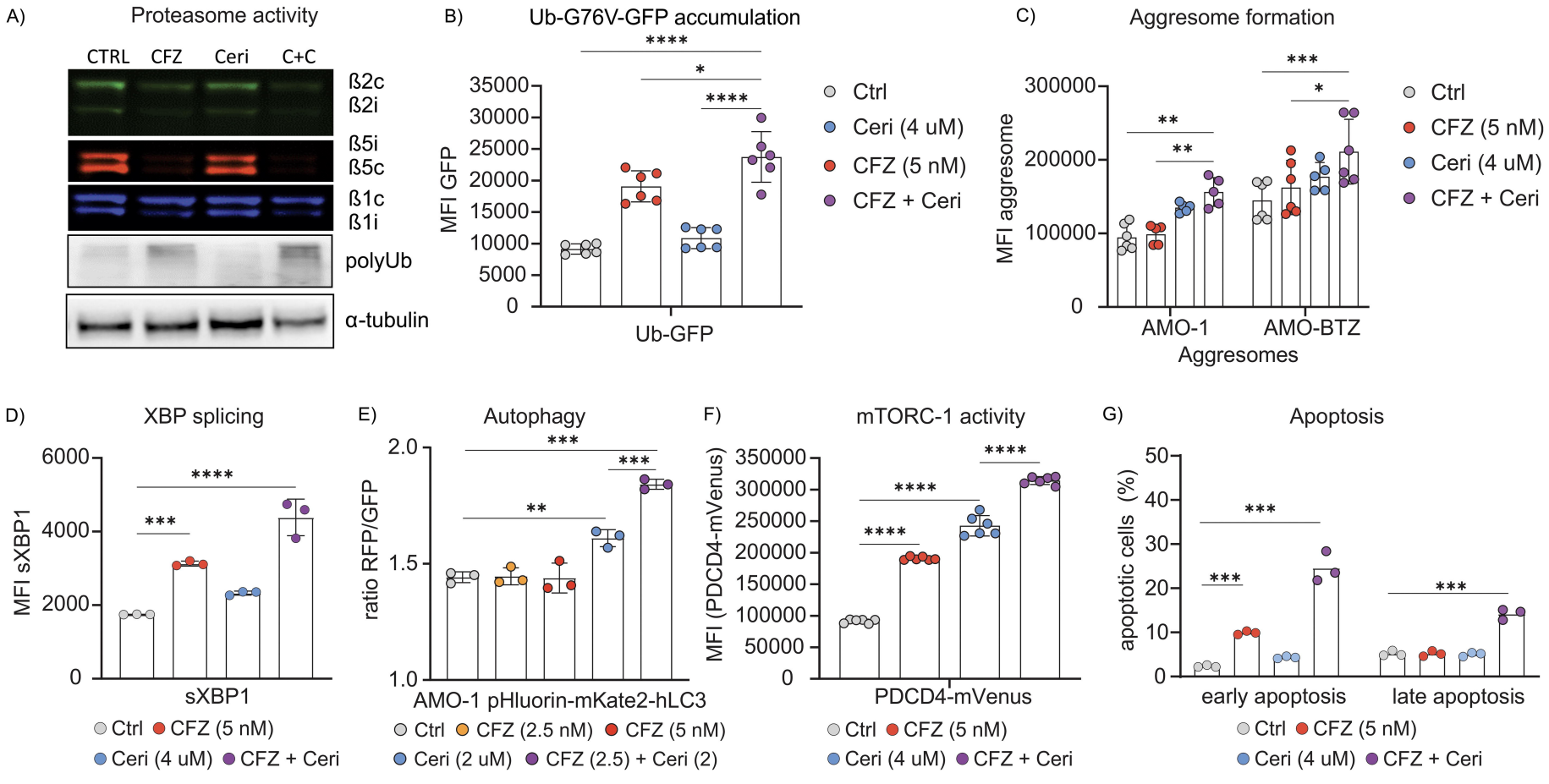
A)
Proteasome activity
CTRL
CFZ
Ceri
C+C
ß2c
ß2i
ß5i
ß5c
ß1c
ß1i
polyUb
α-tubulin
B)
Ub-G76V-GFP accumulation
MFI GFP
Ub-GFP
Ctrl
Ceri (4 uM)
CFZ (5 nM)
CFZ + Ceri
C)
Aggresome formation
MFI aggresome
AMO-1
AMO-BTZ
Aggresomes
Ctrl
CFZ (5 nM)
Ceri (4 uM)
CFZ + Ceri
D)
XBP splicing
MFI sXBP1
sXBP1
Ctrl
CFZ (5 nM)
Ceri (4 uM)
CFZ + Ceri
E)
Autophagy
ratio RFP/GFP
AMO-1 pHluorin-mKate2-hLC3
Ctrl
CFZ (2.5 nM)
CFZ (5 nM)
Ceri (2 uM)
CFZ (2.5) + Ceri (2)
F)
mTORC-1 activity
MFI (PDCD4-mVenus)
PDCD4-mVenus
Ctrl
CFZ (5 nM)
Ceri (4 uM)
CFZ + Ceri
G)
Apoptosis
apoptotic cells (%)
early apoptosis
late apoptosis
Ctrl
CFZ (5 nM)
Ceri (4 uM)
CFZ + Ceri

Figure 6

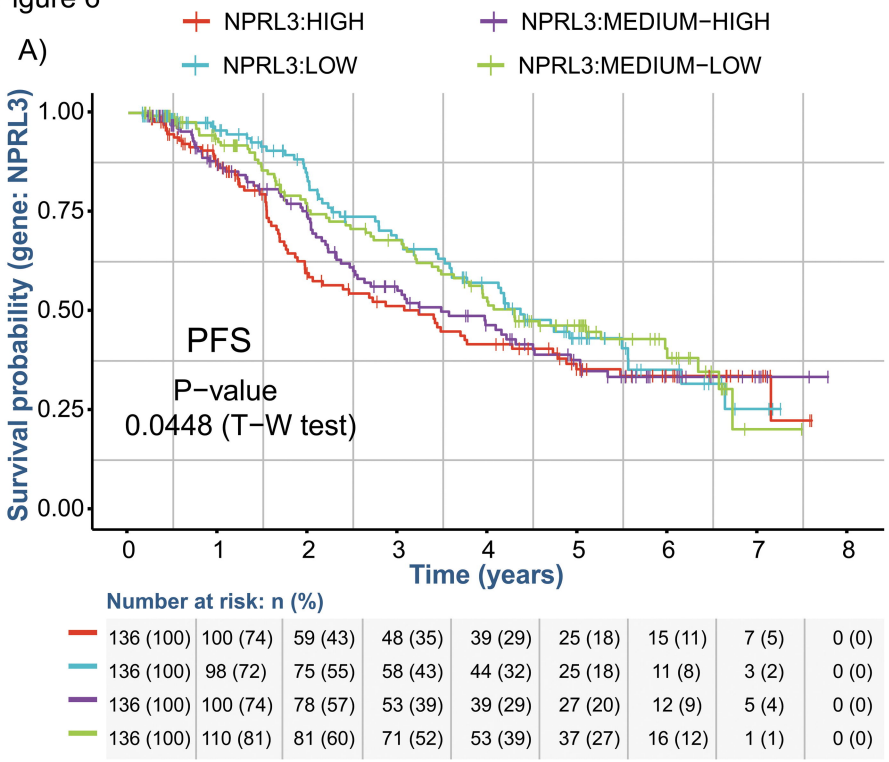
A)
NPRL3:HIGH
NPRL3:MEDIUM−HIGH
NPRL3:LOW
NPRL3:MEDIUM−LOW
Survival probability (gene: NPRL3)
1.00
0.75
0.50
0.25
0.00
PFS
P−value
0.0448 (T−W test)
0
1
2
3
4
5
6
7
8
Time (years)
Number at risk: n (%)
136 (100) 100 (74) 59 (43) 48 (35) 39 (29) 25 (18) 15 (11) 7 (5) 0 (0)
136 (100) 98 (72) 75 (55) 58 (43) 44 (32) 25 (18) 11 (8) 3 (2) 0 (0)
136 (100) 100 (74) 78 (57) 53 (39) 39 (29) 27 (20) 12 (9) 5 (4) 0 (0)
136 (100) 110 (81) 81 (60) 71 (52) 53 (39) 37 (27) 16 (12) 1 (1) 0 (0)

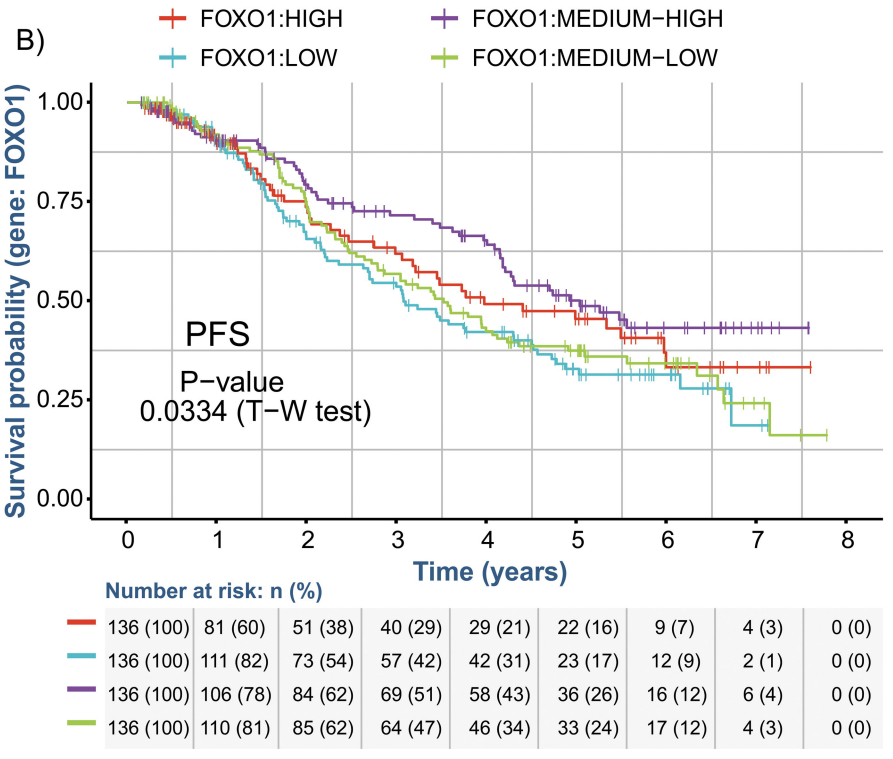
B)
FOXO1:HIGH
FOXO1:MEDIUM−HIGH
FOXO1:LOW
FOXO1:MEDIUM−LOW
Survival probability (gene: FOXO1)
1.00
0.75
0.50
0.25
0.00
PFS
P−value
0.0334 (T−W test)
0
1
2
3
4
5
6
7
8
Time (years)
Number at risk: n (%)
136 (100) 81 (60) 51 (38) 40 (29) 29 (21) 22 (16) 9 (7) 4 (3) 0 (0)
136 (100) 111 (82) 73 (54) 57 (42) 42 (31) 23 (17) 12 (9) 2 (1) 0 (0)
136 (100) 106 (78) 84 (62) 69 (51) 58 (43) 36 (26) 16 (12) 6 (4) 0 (0)
136 (100) 110 (81) 85 (62) 64 (47) 46 (34) 33 (24) 17 (12) 4 (3) 0 (0)

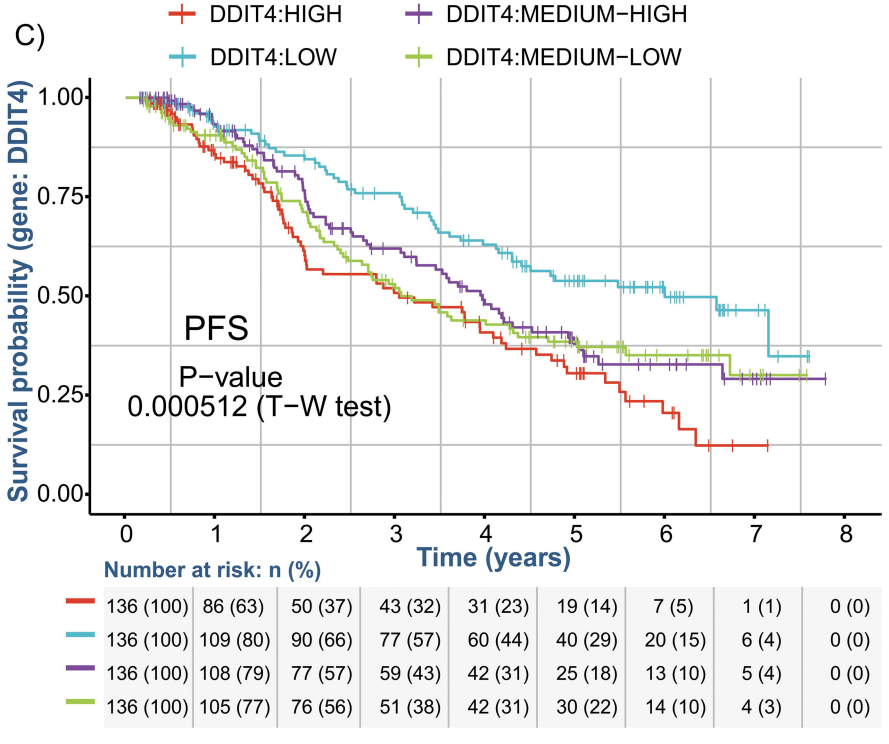
C)
DDIT4:HIGH
DDIT4:MEDIUM−HIGH
DDIT4:LOW
DDIT4:MEDIUM−LOW
Survival probability (gene: DDIT4)
1.00
0.75
0.50
0.25
0.00
PFS
P−value
0.000512 (T−W test)
0
1
2
3
4
5
6
7
8
Time (years)
Number at risk: n (%)
136 (100) 86 (63) 50 (37) 43 (32) 31 (23) 19 (14) 7 (5) 1 (1) 0 (0)
136 (100) 109 (80) 90 (66) 77 (57) 60 (44) 40 (29) 20 (15) 6 (4) 0 (0)
136 (100) 108 (79) 77 (57) 59 (43) 42 (31) 25 (18) 13 (10) 5 (4) 0 (0)
136 (100) 105 (77) 76 (56) 51 (38) 42 (31) 30 (22) 14 (10) 4 (3) 0 (0)

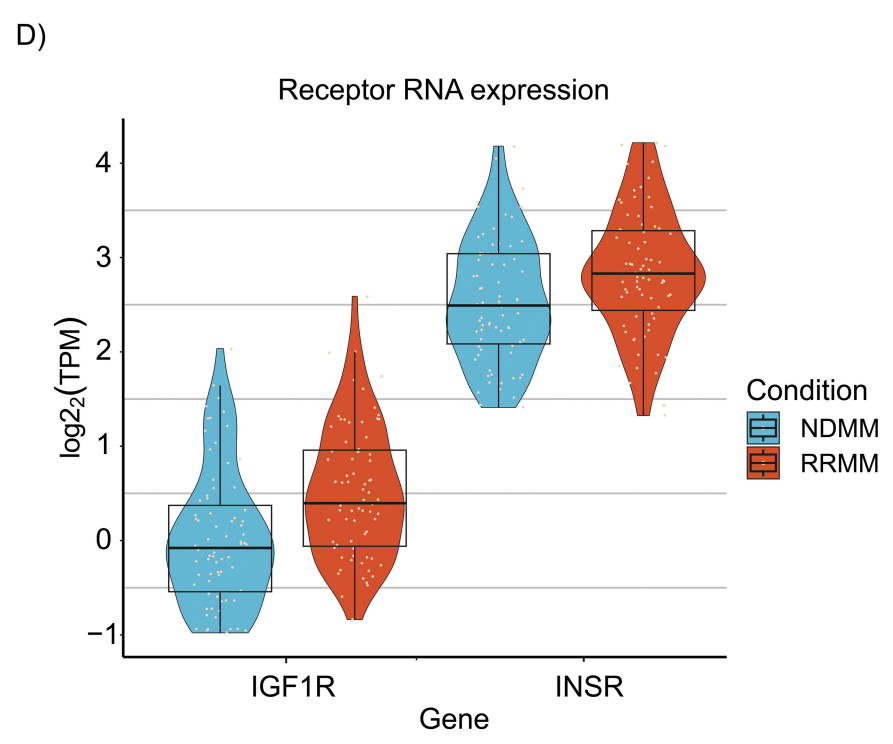
D)
Receptor RNA expression
log2(TPM)
4
3
2
1
0
−1
IGF1R
INSR
Gene
Condition
NDMM
RRMM

SUPPLEMENTARY DATA

SUPPLEMENTARY METHODS

Cell culture

The myeloma cell lines (AMO-1, L363, RPMI-8226 and ARH-77) and their derivatives were maintained in 10% FCS-supplemented RPMI-1640 with 1% penicillin/streptomycin (all Merck/Sigma–Aldrich, Buchs, Switzerland). U2-OS cell line was maintained in 10% FCS-supplemented Dulbecco's Modified Eagle's Medium (DMEM) with 1% penicillin/streptomycin (all Merck/Sigma–Aldrich). Cell lines were routinely tested for mycoplasma contamination using MycoAlert Mycoplasma Detection Kit (Lonza, Basel, Switzerland) and verified by STR-typing (DSMZ, Braunschweig, Germany).

Chemicals

Proteasome inhibitors: bortezomib (PS-341; HY-10227) and carfilzomib (PR-171; HY-10455), ALK-inhibitors: crizotinib (PF-02341066; HY-50878), ceritinib (LDK378; HY-15656), brigatinib (AP-26113; HY-12857), entrectinib (NMS-E628; HY-12678), alectinib (CH5424802; HY-13011), lorlatinib (PF-06463922; HY-12215) and ensartinib (X-396; HY-103714) ; FOXO-1 inhibitor (AS-1842856; HY-100596), IGF-1R/INSR inhibitor (NVP-AEW541; HY-50866), IGF-1R/INSR inhibitor (BMS-536924; HY-10262), were purchased from MedChem Express (Monmouth Junction, NJ, USA).

Viability assays

Cytotoxicity of the treatments in cell lines was assessed using the Cell Counting Kit-8 (CCK-8) colorimetric assay (GLPBio, Montclair, CA, USA). Cells were seeded into clear, flat-bottom 96-well plates and treated with the indicated doses and drug combinations for 48 hours. Following treatment, CCK-8 reagent was added, and absorbance was measured at 492 nm using a Tecan microplate reader (Tecan, Männedorf, Switzerland).

For primary cells, cytotoxicity was evaluated using the CellTiter-Glo luminescence assay (Promega, Madison, WI, USA). Cells were seeded in white, flat-bottom 96-well plates and treated under the same conditions. After 48 hours, luminescence was measured using a Tecan reader.

Dose-response curves and IC_{50} values were generated using non-linear regression analysis. The coefficient of drug interaction (CDI) in the combination treatment was calculated as

previously described.[1] To identify the doses generating the strongest interaction, multiple drug combinations were tested in the indicated cell lines, and only the data showing the lowest CDI for each cell line are presented. CDI values between 0.0 and 0.8 indicate synergistic effects, values between 0.8 and 1.0 suggest additive effects, and values greater than 1.0 indicate antagonism.

Determination of proteasome activity by active site labeling with activity-based probes

Proteasome-specific affinity-based probes, each targeting a specific proteasome subunit, were used to evaluate the activity of all constitutive and immunoproteasome subunits as described.[2] In brief, equal amounts of total protein were resolved by SDS-PAGE using bis-tris 12% gels (Thermo Fisher Scientific, MA, USA), and labeled active β-subunits were directly visualized in the gel using Fusion Solo S (Vilber Lourmat, France).

Western blots

Briefly, samples were lysed with lysis buffer, and 20 µg of protein per lane was separated by SDS-PAGE on Bis-Tris 10% gels (Thermo Fisher Scientific, MA, USA). After SDS-PAGE, proteins were transferred onto PVDF membranes. The membranes were then blocked with RotiBlock (Roth, Germany) and incubated with primary antibodies. The following day, the membranes were washed, incubated with secondary antibodies, and the chemiluminescence signal was acquired after treatment with the HCL substrate using the Fusion S Solo camera (Vilber Lourmat, France).

Antibody	**Source**	**ID**
HSP70 (rabbit)	Invitrogen	#PA1-014A; RRID:AB_559362
HSPA5 (GRP78, BiP) (mouse)	Invitrogen	#MA3-006; RRID:AB_325454
phospho-p70 S6 Kinase (rabbit)	Cell Signaling Technology	#9204; RRID:AB_2265913
p70 S6 Kinase (rabbit)	Cell Signaling Technology	#9202; RRID:AB_331676
phospho-S6 Ribosomal protein (rabbit)	Cell Signaling Technology	#4858; RRID:AB_916156
S6 Ribosomal protein (rabbit)	Cell Signaling Technology	#2217; RRID:AB_331355
Ub-K48 Recombinant Rabbit Monoclonal Antibody (ARC0811)	Invitrogen	#MA5-35382; RRID:AB_2849283
HRP-conjugated β-actin (mouse)	Proteintech	#60008; RRID:AB_2819183
HRP-conjugated α-tubulin (mouse)	Proteintech	#66031; RRID:AB_2687491
Peroxidase AffiniPure Goat Anti-Rabbit IgG	JacksonImmunoResearch	#111-035-003; RRID:AB_2313567
Peroxidase AffiniPure™ Sheep Anti-Mouse IgG	JacksonImmunoResearch	#515-035-003; RRID:AB_2340295

RNA seq data analysis of MM cell lines

RNA sequencing data from multiple MM cell lines were obtained from publicly available sources under the accession number GSE160572, as previously described.[3]

RNA sequencing after drug treatment and data analysis

AMO-1 cells were treated for 8 h with ceritinib (4μM), carfilzomib (5 nM) or drug combinations. Subsequently, the cells were washed with PBS and snap-frozen in liquid nitrogen. RNA sequencing analysis was performed by the BGI Tech Solutions (Hong Kong) using NovaSeq (Illumina). Samples were sequenced using paired-end 75 bp reads; NEBNext Ultra II Directional RNA Library Prep Kit for Illumina + polyA selection (New England Biolabs, Ipswich, MA, USA). The obtained data passed quality control. Differential gene expression was calculated by DESeq2.[4] Differently expressed genes with adjusted p value < 0.05 were taken into further analyses. All data related to differentially expressed genes between treatment conditions are presented in the **Supplementary Table S6.**

Kinase inhibitor selectivity data

Kinase inhibitor selectivity data was retrieved from ChEMBL version 30. All activity data available for the clinical inhibitors were downloaded through the web interface and aggregated on a protein level using KNIME Analytics Platform (version 4.5). Proteins were then sorted based on the count of assigned 'ACTIVE' in ChEMBL, corresponding to any determined inhibition constant for the inhibitor protein pair. This resulted in 33 proteins for which at least 3 of 6 inhibitors were known to be active, with ALK as expected targeted by all 6.

Multiple Myeloma Research Foundation CoMMpass dataset analysis

Multiple Myeloma Research Foundation (MMRF) provided an access to the CoMMpass study. Data were accessed via the MMRF Researcher Gateway (IA18 release) on 20th of March, 2020. The salmon aligned untraded transcripts, survival data and patients' information was used to analyze the expression of INSR, IGF-1R, ALK, FLT3, BLK, LCK, ZAP70, FES, BTK, SRC, NRPL2, NRPL3, TSC1, TSC2, DDIT4, FOXO1 and DDIT4 in plasma cells from 544 MM patients at the time of diagnosis. The data was filtered to exclude patients that died from unrelated causes, had illnesses that were reported to interfere with the study assessment, were not complaint with the study procedure, were removed from the study due to untreated health problems or had a stem-cell transplant done after the first line of therapy while including only patients with ages between 45 and 85 years. The majority of patients were treated with

proteasome inhibitors. For INSR, IGF1R, NPRL2, NPRL3, DDIT4, FOXO1 and PDCD4, the association with overall survival and progression-free survival was estimated using Kaplan-Meier survival analysis,[5] the statistical significance being tested through the Tarone-Ware test.[6] Gene expression levels were stratified into four groups based on quartile splits, allowing for a comparison of survival outcomes across different expression levels. For extracting the expression level information, raw gene counts were normalized using the DESeq2 pipeline For these analyses, the following R packages were used: readr,[7] stringr,[8] DESeq2,[4] ggplot2,[9] survival,[10] tidyverse,[11] xlsx,[12] clusterProfiler,[13] survminer,[14] coin[15] and edgeR.[16]

Relapsed/refractory dataset analysis

A bulk RNA-seq data from RRMM patients from University Hospital Würzburg was used to analyze the expression changes in plasma cells obtained from 75 MM patients at relapse, as previously described.[17] The study was approved by the Internal Review Board at the University hospital of Würzburg (Wü8/21) and adhered to the tenets of the Declaration of Helsinki. RRMM was defined as per current IMWG criteria.[18] To compare expression of INSR and IGF1R between newly diagnosed patients from CoMMpass and dataset of RRMM from Wurzburg, first a Spearman correlation was computed between the 2 studies datasets and the top 75 samples with the highest median correlation from the MMRF datasets with respect to the Wurzburg dataset were selected. MMRF and Wurzburg datasets were aggregated together and filtered to exclude entries with a total sum in all experiments below 400 and that have more than 3 missing values. Moreover, entries with TPM values above 10000 in at least one experiment were removed to help normalize the distributions (these were considerable outliers). An initial list of stable genes was extracted by performing a Kolmogorov-Smirnov test on the log-transformed data, corrected using the BH method for multiple testing, and selecting the genes with an FDR higher than 0.25 (around 400 genes out of 9500). These genes were used as the baseline information for RUVg batch correction algorithm on the normal scale using only one factor of unwanted variation (k). Afterward, the data was normalized using the median of ratios normalization on the log2 scale. Lastly, a limma trend analysis pipeline was applied to identify differentially expressed elements. This consists of estimating the weights for each sample before performing the linear modeling. An intensity-dependent prior trend was used as well as a robust identification of the prior variance and degrees of freedom against outliers. A gene was deemed as differentially expressed if it had an FDR value below 10^{-5} and an absolute log2FC value above 0.75.

Cancer Dependency Map data analysis

The expression and dependency scores of BTK (Bruton Tyrosine Kinase), IGF-1R (Insulin-Like Growth Factor 1 Receptor), INSR (Insulin Receptor), and SRC (SRC Proto-Oncogene, Non-Receptor Tyrosine Kinase) genes were analyzed using data from the DepMap Public 24Q4 dataset. Gene expression levels were assessed using RNA-seq-derived transcripts per million (TPM), normalized across cell lines. Gene dependency was evaluated using CRISPR-Cas9 loss-of-function screening data, specifically the Chronos dependency scores, where lower scores indicate stronger dependency. Analysis was conducted across a panel of 24 MM cell lines.

Untargeted metabolomics analysis

AMO-1 cells were treated for 8 h with ceritinib (4μM), carfilzomib (5 nM) or drug combinations. Subsequently, the cells were washed with PBS and snap-frozen in liquid nitrogen. Untargeted metabolomics analysis was performed by the BGI Tech Solutions (Hong Kong). A Waters UPLC I-Class Plus (Waters, USA) tandem Q Exactive high-resolution mass spectrometer (UPLS-MS) (Thermo Fisher Scientific, USA) was used for separation and detection of metabolites. Data quality control was ensured and is described in detail in supplementary methods. Data pre-processing was performed using metaX,[19] to obtain all forms of compounds and their intensities for the next step of data analysis. Classification and functional annotation of the identified metabolites were performed according to their KEGG ID and HMDB ID, and search in respective databases. For the comparison of two groups (treatment vs. control), univariate analysis was used: fold change (ratio between two groups in analysis) was calculated, and the p value was obtained by the t-test. Only metabolites with a p-value < 0.05 and FC ≥ 1.2 or ≤ 0.83 were considered statistically different. For better visualization, the data are presented as log2 (FC) values. All metabolites identified in the treatment conditions and compared between the conditions are presented in the **Supplementary Table S10.** Enrichment analysis of statistically different metabolites was performed using the MetaboAnalyst analysis toolkit.[20]

PamGene Kinase screening

The PamGene assays measure kinase activity in cell and tissue lysates by measuring the phosphorylation of peptide representations of kinase targets/ substrates (referred hereafter as phosphosites) that are immobilized on the PamChip® microarrays (PamGene International, s-Hertogenbosch, The Netherlands). Two types of PamChip® microarrays have been used to evaluate the activity of ceritinib in AMO-1 cells following 30 min incubation with 4μM ceritinib;

one, which evaluates phosphosites of 196 protein tyrosine kinase (PTK) and the other one, which evaluates phosphosites of 144 serine/threonine kinase (STK). In brief, whole-cell lysates were prepared using lysis buffer that contained inhibitors of proteases and phosphatases and were stored immediately in a −80 °C freezer. Protein quantification was performed with the bicinchoninic acid assay according to the manufacturer's instructions (BCA; Merck KGaA, Darmstadt, Germany). Per array 5 µg of protein and 400 µM ATP were applied. Sequence-specific peptide tyrosine and serin–threonin phosphorylation were detected by the fluorescein-labeled antibody PY20 (Exalpha, Maynard, MA, USA) and a CCD camera using the Evolve software (1200PTKlysv04.PS12Protocol; PamGene International). Data were analyzed using the Bio Navigator software (PamGene International). To identify significant differences in PTK phosphosites between control and ceritinib-treated cells, an ANOVA with Dunnett post-test was used, for analysis of differences in STK phosphosites, LIMMA was applied.

Apoptosis determination

The AMO-1 cells were exposed to the indicated drugs for 24 h. The cells were washed and stained using an Annexin V/FITC Detection Kit (Vazyme Biotech, Nanjing, China), according to the manufacturer's instructions. The fluorescence intensity of the cells was analyzed using a BD LSR Fortessa cell analyzer (BD Biosciences, New Jersey, USA). The data were analyzed using the BD FACS DIVA Software (BD Biosciences).

Evaluation of autophagic flux

AMO-1 cells were transduced with a lentiviral vector expressing the pHluorin-mKate2-hLC3 construct (FUGW-PK-hLC3, RRID:Addgene_61460, kindly provided by Isei Tanida[21]), enabling simultaneous quantitative assessment of autophagosome and lysosome formation. This system leverages the pH-sensitive quenching of GFP within lysosomes, combined with the pH-stable fluorescence of mKate2. As a result, autophagosomes appear yellow (due to combined GFP and RFP signals), while lysosomes appear red (due to loss of GFP fluorescence and persistence of RFP), allowing differentiation based on the RFP/GFP fluorescence ratio. Lentivirus production followed the protocol described above. Transduced cells were sorted based on stable RFP expression and subcloned. Single-cell-derived clones with the highest RFP signal were selected for subsequent experiments. To measure autophagic flux, cells were treated with the indicated drugs for 8 hours, washed with PBS, and analyzed for RFP and GFP fluorescence using a BD LSR Fortessa cell analyzer (BD Biosciences). Data were processed and analyzed using BD FACSDiva Software (BD Biosciences).

Analysis of UPR induction

AMO-1 cells were equipped with ER-stress sensor, an XBP1 splicing fluorescent reporter with mNeonGreen[22] (RRID:Addgene_115968; a gift from David Andrews). Lentivirus was produced as described above. Transduced cells were sorted for fluorescence intensity after ER stress and subcloned. The single-cell-derived clones with the highest positivity were used in the experiments.

To measure UPR induction, the cells were treated with the drugs for 8 h, washed with PBS and the fluorescence intensity of the reporters was determined using a BD LSRFortessa cell analyzer (BD). The data were analyzed using the FACSDiva Software (BD Biosciences).

Analysis of mTORC1 activity

AMO-1 cells were equipped with mVenus-TOSI, a fluorescent reporter for mTORC1 signaling (monitoring PDCD4 degradation, RRID:Addgene_172491, a gift from David Scadden) using retroviral transduction. Retrovirus was produced using pUMVC and pCMV-VSV-G plasmids (RRID:Addgene_8448 and RRID:Addgene_8454, both gifts from Bob Weinberg) in HEK-293-LentiX cell line (Clontech/Takara Bio; Saint-Germain-en-Laye, France). Transduced cells were sorted for fluorescence intensity and subcloned. The single-cell-derived clones with the highest positivity were used in the experiments.

To measure mTORC1 inhibition, the cells were treated with the drugs for 12 h, washed with PBS and the fluorescence intensity of the PDCD4-reporter was determined using a BD LSRFortessa cell analyzer (BD Biosciences). The data were analyzed using the FACSDiva Software (BD Biosciences).

Aggresome formation

Formation of aggresomes, inclusion bodies of aggregated, misfolded proteins that form when the ubiquitin-proteasome protein-degradation machinery is overwhelmed, was evaluated 20 h after treatment using the PROTEOSTAT® Aggresome Detection Kit (Enzo Life Sciences, Farmingdale, NY, USA), according to the manufacturer´s recommendations. The intensity of fluorescence was determined using a BD LSRFortessa cell analyzer (BD Biosciences). The data were analyzed using the FACSDiva Software (BD Biosciences).

Analysis of proteasome function by Ub-G76V-GFP

AMO-1 cells were stably expressing Ub-G76V-GFP were generated previously.[23] Accumulation of GFP fluorescence in cells 12 h after respective treatment was acquired using a BD LSRFortessa cell analyzer (BD Biosciences). The data were analyzed using the FACSDiva Software (BD Biosciences).

Generation of U-2 OS cells with full FOXO1-Clover

U-2 OS cells were equipped with fluorescently-tagged FOXO-1 construct using lentiviral transduction, as described above. pLenti-FoxO1-Clover (RRID:Addgene_67759, a gift from Peter Rotwein), allows assessment of Akt activity in single cells[24] using FoxO-1, a well-characterized Akt kinase substrate.[25] The transduced cells were enriched for GFP positivity and subcloned. The single-cell-derived clones with stable and uniform GFP fluorescence were further used. To identify nuclear translocation of FOXO-Clover, cells were equipped with nuc-mCherry-pTRIP (RRID:Addgene_163520, a gift from Thomas Weber).

Incucyte measurement

Real-time monitoring of FOXO-1 localization was performed using the Incucyte® S3 Live-Cell Analysis System (Sartorius, Göttingen, Germany), following the Real-Time Kinetic Analysis of Akt Activity protocol provided by Sartorius. Cells were imaged and analyzed over a 12-hour period every hour. In this setup, nuclear regions were identified via the mCherry signal, while FOXO-1 localization was tracked through the Clover (GFP) signal. Quantification of nuclear FOXO-1 was performed by measuring the GFP fluorescence intensity within the mCherry-defined nuclear area. Translocation was expressed as 1 - normalized nuclear GFP intensity relative to time 0, indicating FOXO-1 ratio in nucleus to the cytoplasm over time.

Quantification and statistical analysis

Statistical analysis was performed as indicated in specific method description or in figure legends. A p value < 0.05 was considered to indicate statistical significance.

Unless otherwise specified, all data were evaluated in GraphPad Prism v10 (GraphPad Software, La Jolla, CA). Graphical abstract was generated using CorelDRAW Graphics Suite (Alludo, 2025), v 2018.

SUPPLEMENTARY FIGURES

Figure S1: Cytotoxicity of ceritinib in combination with proteasome inhibitors in the AMO-1 model, represented as a decrease in viability relative to control cells.

(A, B, C) Cytotoxicity of ceritinib in combination with bortezomib in AMO-1, AMO-BTZ and AMO-CFZ cells.

(D, E, F) Cytotoxicity of ceritinib in combination with carfilzomib in AMO-1, AMO-BTZ and AMO-CFZ cells.

Cell viability was assessed 48 h after continuous treatment. Data represent the mean ± SD from at least 3 independent experiments. The coefficient of drug interaction (CDI) for the combination treatments was calculated and is presented in Table 1.

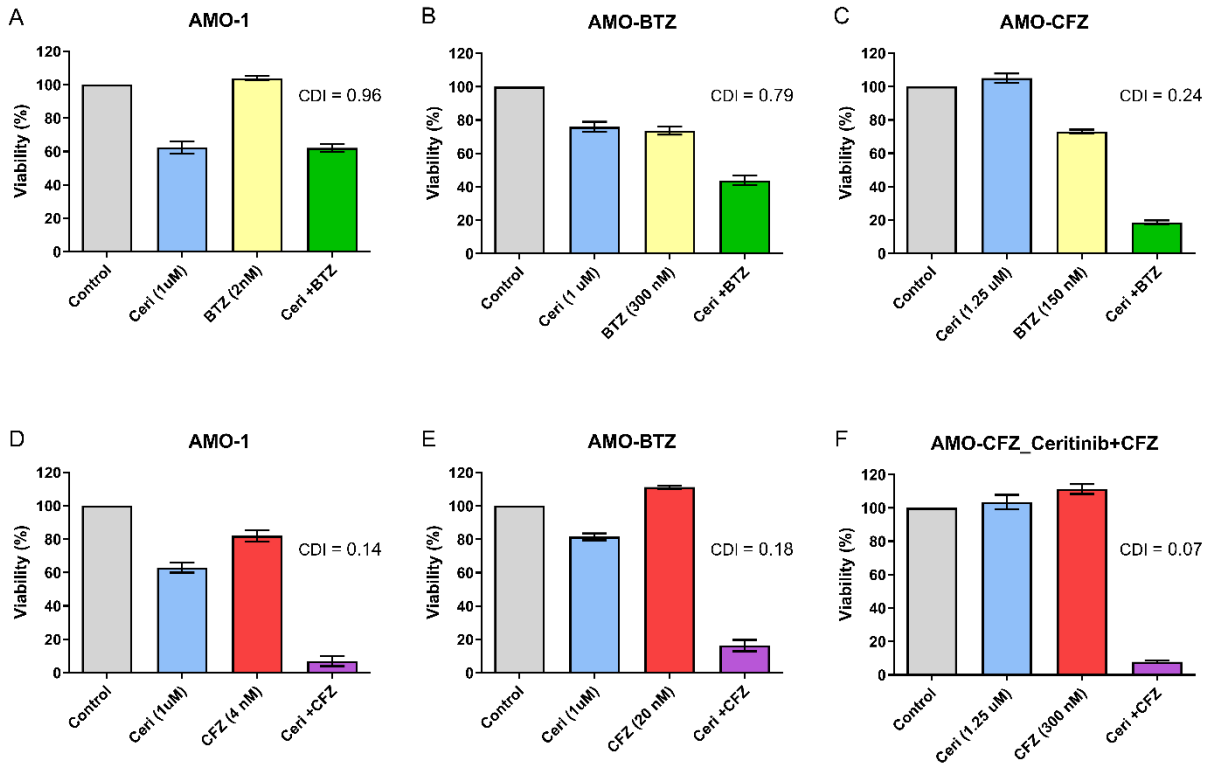

BTZ: bortezomib; Ceri: ceritinib; CFZ: carfilzomib.

Figure S2: Cytotoxicity of ceritinib in combination with proteasome inhibitors in the L363 model, represented as a decrease in viability relative to control cells.

(A, B, C) Cytotoxicity of ceritinib in combination with bortezomib in L363, L363-BTZ and L363-CFZ cells.

(D, E, F) Cytotoxicity of ceritinib in combination with carfilzomib in L363, L363-BTZ and L363-CFZ cells.

Cell viability was assessed 48 h after continuous treatment. Data represent the mean ± SD from at least 3 independent experiments. The coefficient of drug interaction (CDI) for the combination treatments was calculated and is presented in Table 1.

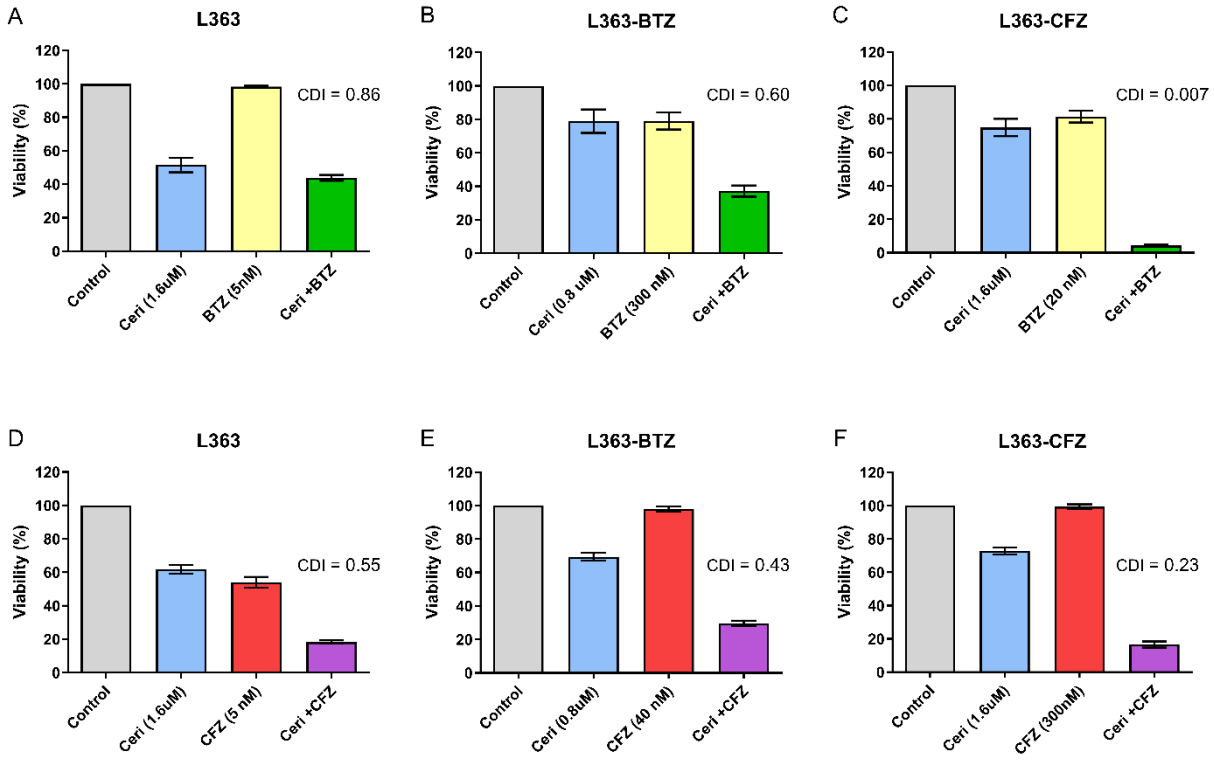

BTZ: bortezomib; Ceri: ceritinib; CFZ: carfilzomib.

Figure S3: Cytotoxicity of ceritinib in combination with proteasome inhibitors in the ARH-77 model, represented as a decrease in viability relative to control cells.

(A, B, C) Cytotoxicity of ceritinib in combination with bortezomib in ARH-77, ARH-BTZ and ARH-CFZ cells.

(D, E, F) Cytotoxicity of ceritinib in combination with carfilzomib in ARH-77, ARH-BTZ and ARH-CFZ cells.

Cell viability was assessed 48 h after continuous treatment. Data represent the mean ± SD from at least 3 independent experiments. The coefficient of drug interaction (CDI) for the combination treatments was calculated and is presented in Table 1.

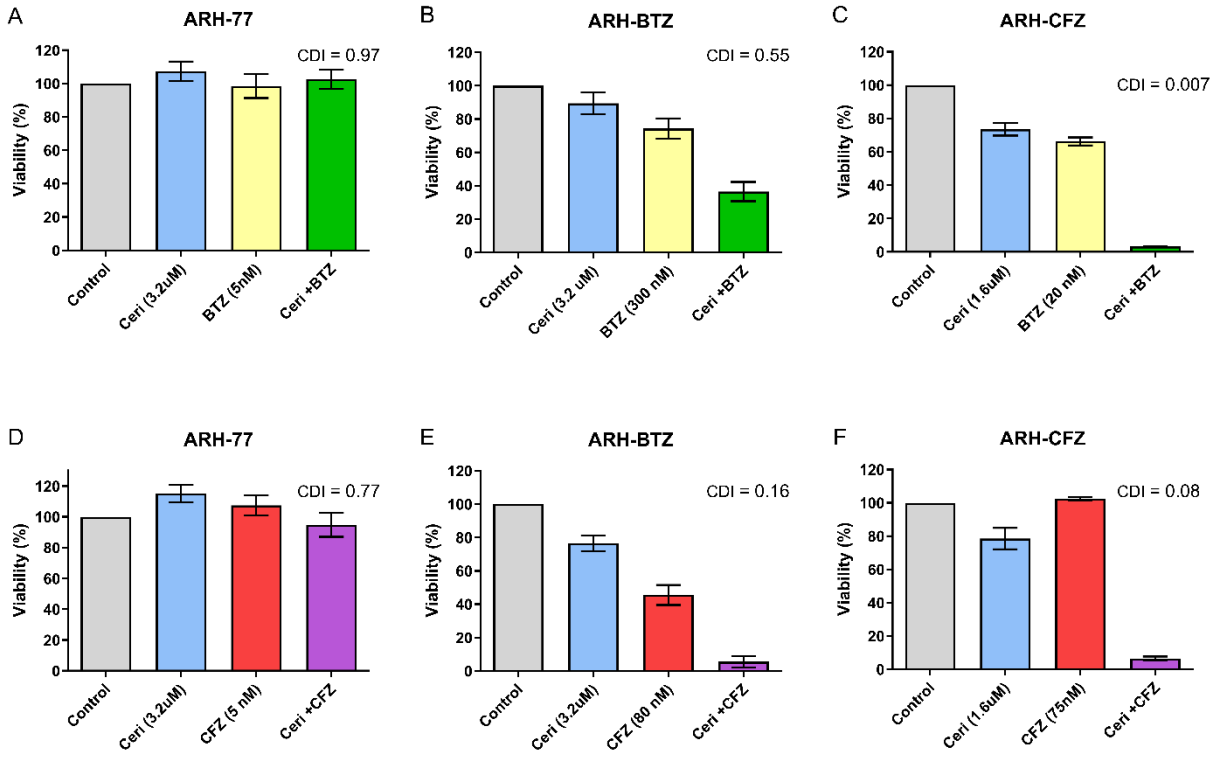

BTZ: bortezomib; Ceri: ceritinib; CFZ: carfilzomib.

Figure S4: Cytotoxicity of ceritinib in combination with proteasome inhibitors in the RPMI-8226 model, represented as a decrease in viability relative to control cells.

(A, B, C) Cytotoxicity of ceritinib in combination with bortezomib in RPMI-8226, RPMI-BTZ and RPMI-CFZ cells.

(D, E, F) Cytotoxicity of ceritinib in combination with carfilzomib in RPMI-8226, RPMI-BTZ and RPMI-CFZ cells.

Cell viability was assessed 48 h after continuous treatment. Data represent the mean ± SD from at least 3 independent experiments. The coefficient of drug interaction (CDI) for the combination treatments is presented in Table 1.

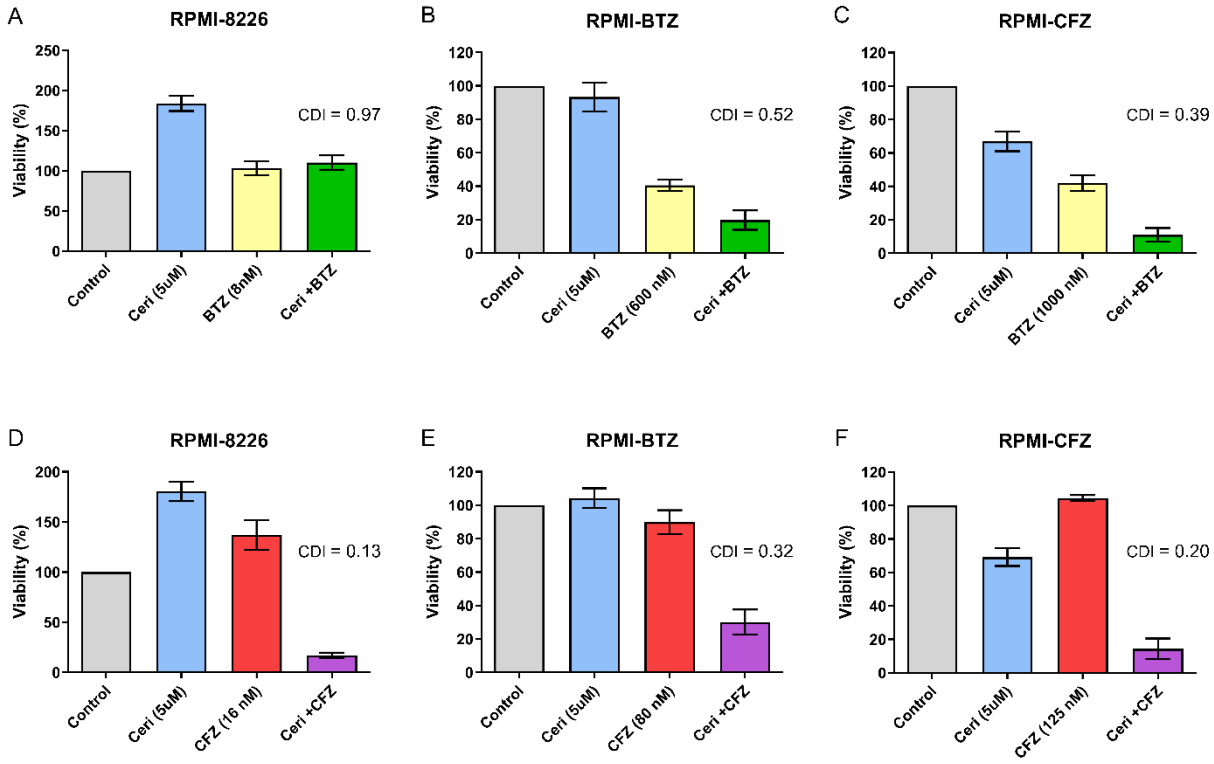

BTZ: bortezomib; Ceri: ceritinib; CFZ: carfilzomib.

Figure S5: Effect of ceritinib, carfilzomib and their combination on mice well-being.

NSG mice were injected intrafemorally with AMO-BTZ cells. Seven days after orthotopic implantation, treatment was initiated with ceritinib (25 mg/kg, orally, 5 days/week), carfilzomib (4 mg/kg, intravenously, 2 days/week), or their combination. Captisol was used as the vehicle control. Mice were treated for 2 weeks and monitored for changes in **(A)** body weight, **(B)** blood glucose levels, and **(C)** hemoglobin levels. Statistical significance was tested with two-way ANOVA and Tukey´s posttest, no significant differences were obtained.

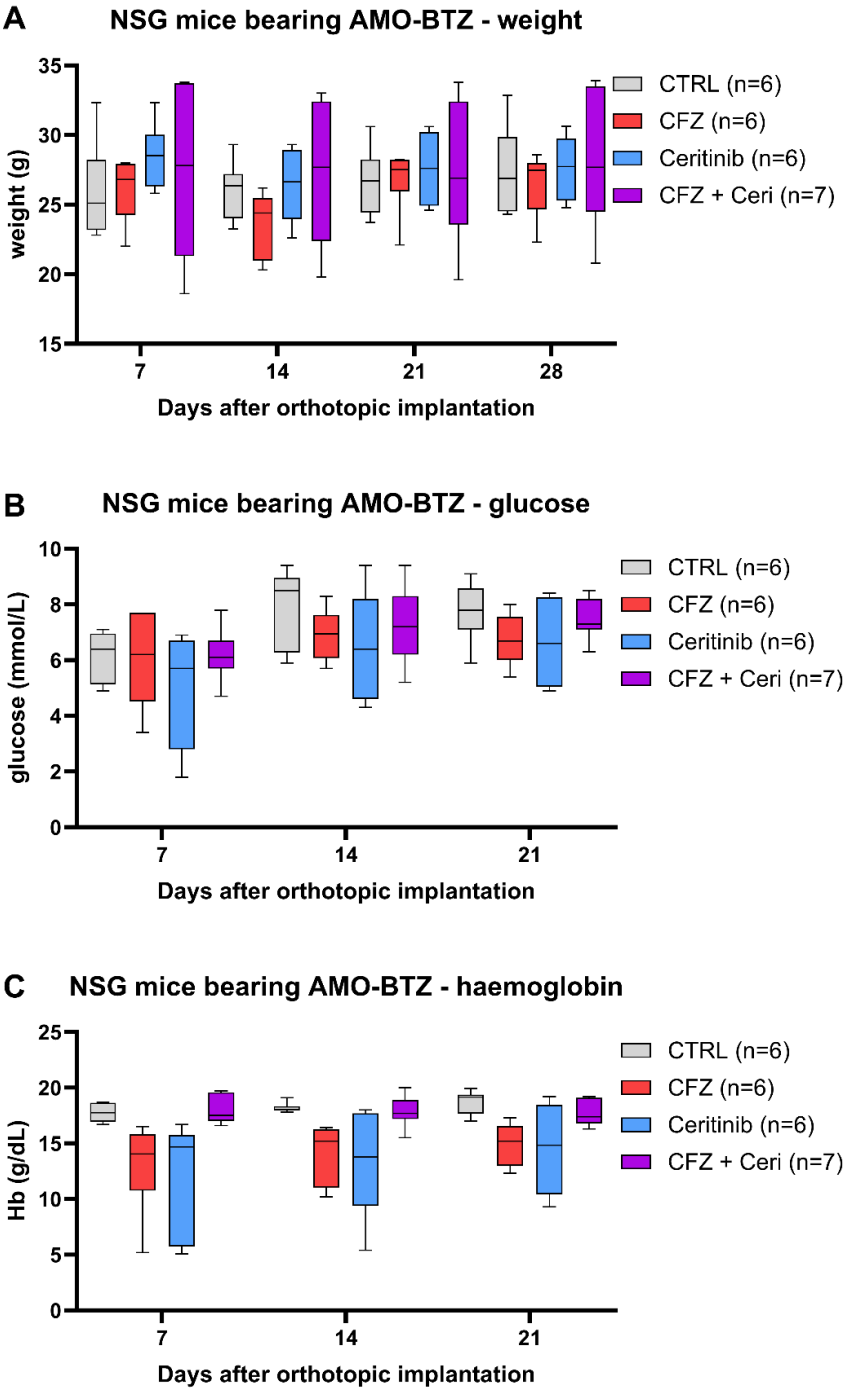

Ceri: ceritinib; CFZ: carfilzomib; CTRL: vehicle control (Captisol); Hb: haemoglobin; NSG: NOD/Scid gamma

Figure S6: Expression of kinases in MM cell lines.

Violin plot representing expression of kinases identified to be candidates for ceritinib inhibition in a set of MM cell lines (AMO-1, AMO-BTZ, AMO-CFZ, L363, L363-BTZ, L363-CFZ, RPMI-8226 and RPMI-BTZ). Data represent FPKM (Fragments Per Kilobase Million) values.

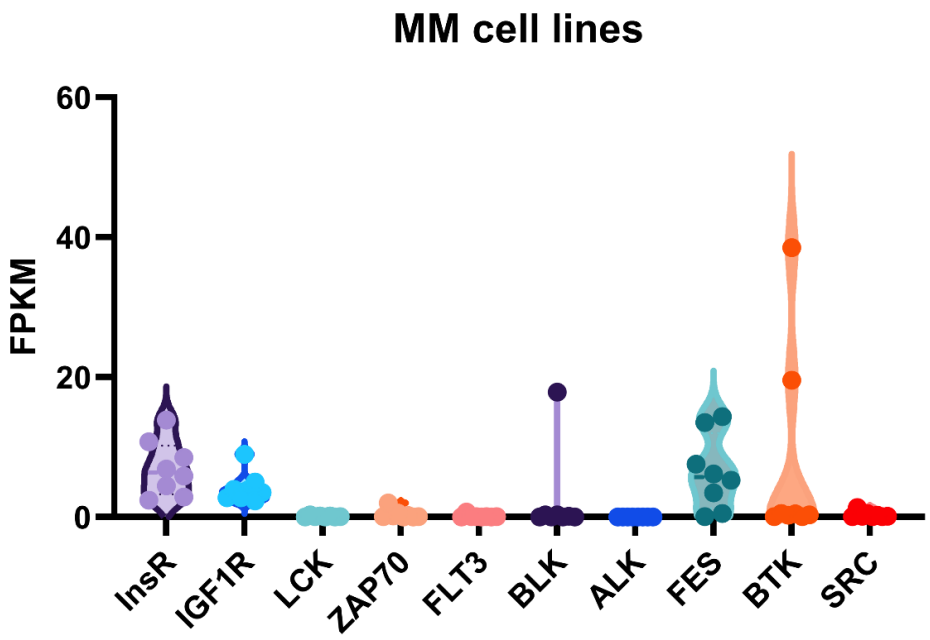

ALK: Anaplastic Lymphoma Receptor Tyrosine Kinase; BLK: B Lymphoid Tyrosine Kinase; BTK: Bruton Tyrosine Kinase; FES: FES Proto-Oncogene, Tyrosine Kinase; FLT3: Fms Related Receptor Tyrosine Kinase 3; IGF-1R: Insulin Like Growth Factor-1 Receptor; INSR: Insulin Receptor; LCK: LCK Proto-Oncogene, Src Family Tyrosine Kinase; SRC: SRC Proto-Oncogene, Non-Receptor Tyrosine Kinase; ZAP70: Zeta Chain Of T Cell Receptor Associated Protein Kinase 70.

FPKM: Fragments Per Kilobase Million

Figure S7: Expression and dependency on putative targets of ceritinib, obtained from Cancer Dependency Map.

(A) Expression of INSR, IGF-1R, BTK and SRC in 24 MM cell lines.

(B) Dependency on INSR, IGF-1R, BTK and SRC in 24 MM cell lines. For dependency, the lower is Gene dependency score, the more essential is the gene for viability. List of cell lines and expression of genes is available in Supplementary Table S4.

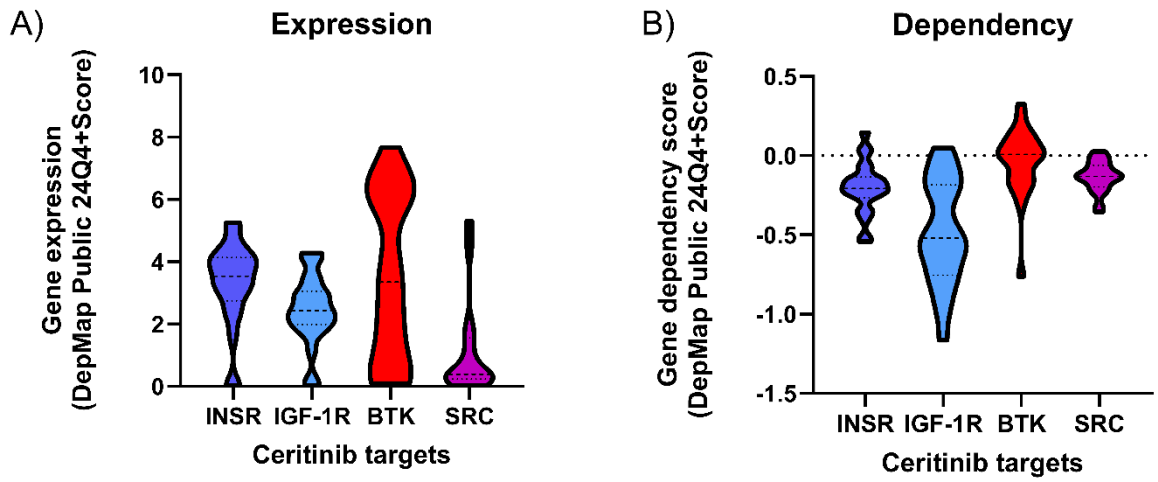

BTK: Bruton Tyrosine Kinase; IGF-1R: Insulin Like Growth Factor-1 Receptor; INSR: Insulin Receptor; SRC: SRC Proto-Oncogene, Non-Receptor Tyrosine Kinase

Figure S8: Cytotoxicity of ceritinib in combination with IGF-1R/INSR inhibitors in MM cells, represented as a decrease of viability relative to control cells.

(A-D) Cytotoxicity of ceritinib in combination with IGF-1R/INSR inhibitor NVP-AEW541 in AMO-1 (A), AMO-BTZ (B), AMO-CFZ (C) and L363 (D) cells.

(E-H) Cytotoxicity of ceritinib in combination with IGF-1R/INSR inhibitor BMS-236924 in AMO-1 (E), AMO-BTZ (F), AMO-CFZ (G) and L363 (H) cells.

In all experiments, viability was assessed 48 hours post continuous treatment. Data represent the mean ± SD of at least 3 independent experiments.

The coefficient of drug interaction (CDI) for the combination treatments was calculated.

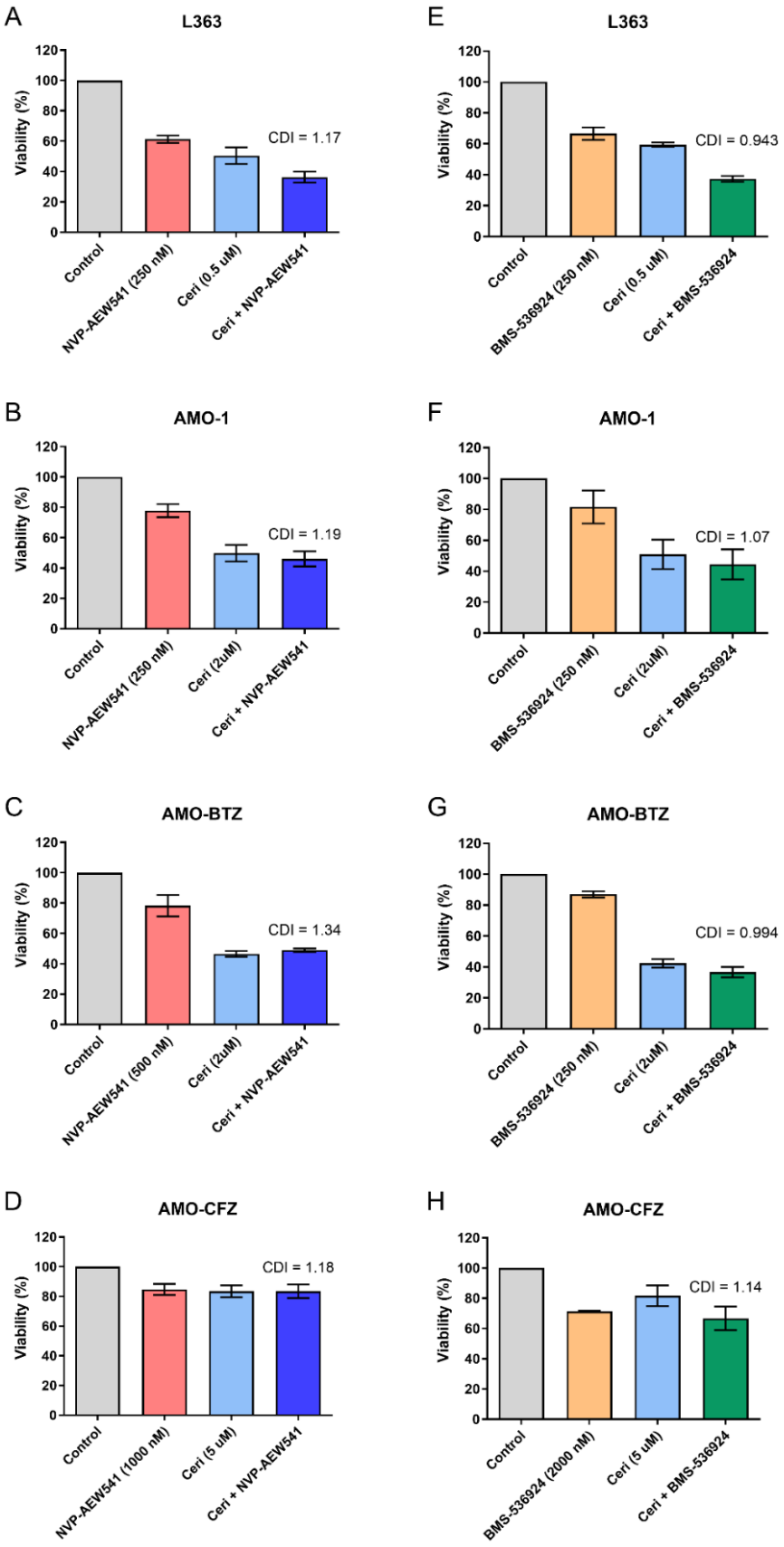

BTZ: bortezomib; CFZ: carfilzomib; IGF-1R: Insulin Like Growth Factor-1 Receptor; INSR: Insulin Receptor

Figure S9: Phosphorylation of p70 S6 kinase and ribosomal protein S6.

Quantification of changes in phosphorylation of p70 S6 kinase (p70S6K) and ribosomal S6 protein in AMO-1 cells following western blot analysis, complementing Figure 3G. Data represent mean ± SD of three independent experiments. Statistical significance was determined by one-way ANOVA with Tukey's multiple comparisons test: *p < 0.05, **p < 0.01, ***p < 0.001, ****p < 0.0001.

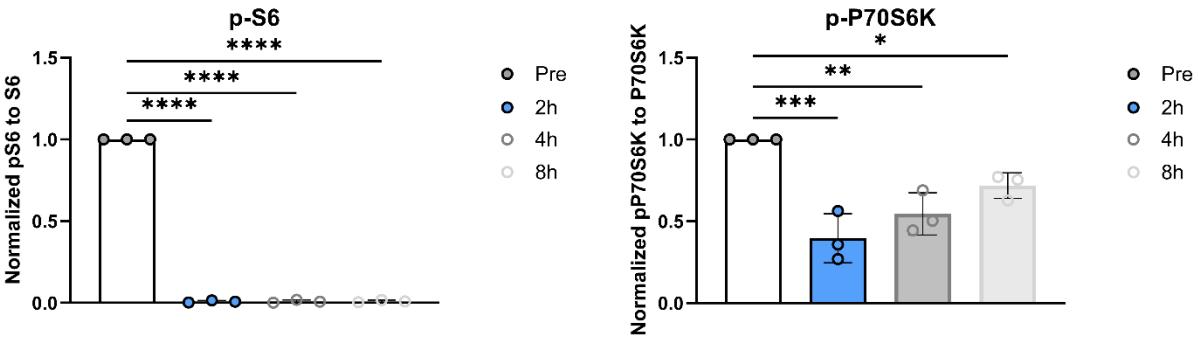

Figure S10: GSEA of ceritinib, carfilzomib, and combination treatments. Enrichment plot showing significantly deregulated biological processes, based on GSEA followed by GO BP classification, in AMO-1 cells 8 hours after treatment with 4 μM ceritinib.
(A) GSEA enrichment plot showing negative enrichment of the E2F target gene set following ceritinib treatment.
(B) Heatmap illustrating the leading-edge deregulated genes (log2 FC ≥ -3 for ceritinib treatment) under the control of the E2F transcription factor.
(C) Enrichment plot depicting significantly deregulated biological processes in AMO-1 cells 8 hours after treatment with 5 nM carfilzomib, based on GSEA and GO BP classification.
(D) GSEA enrichment plot showing positive enrichment of the FOXO1 target gene set following ceritinib treatment.
(E) Enrichment plot showing significantly deregulated biological processes in AMO-1 cells 8 hours after treatment with the combination of 4 μM ceritinib and 5 nM carfilzomib, based on GSEA and GO BP classification.
(F) Heatmap illustrating the leading-edge deregulated genes (log2 FC ≥ 3 for ceritinib treatment) under the regulation of the FOXO1 transcription factor.
(G) Heatmap of leading-edge genes associated with the autophagy biological process identified through GSEA.

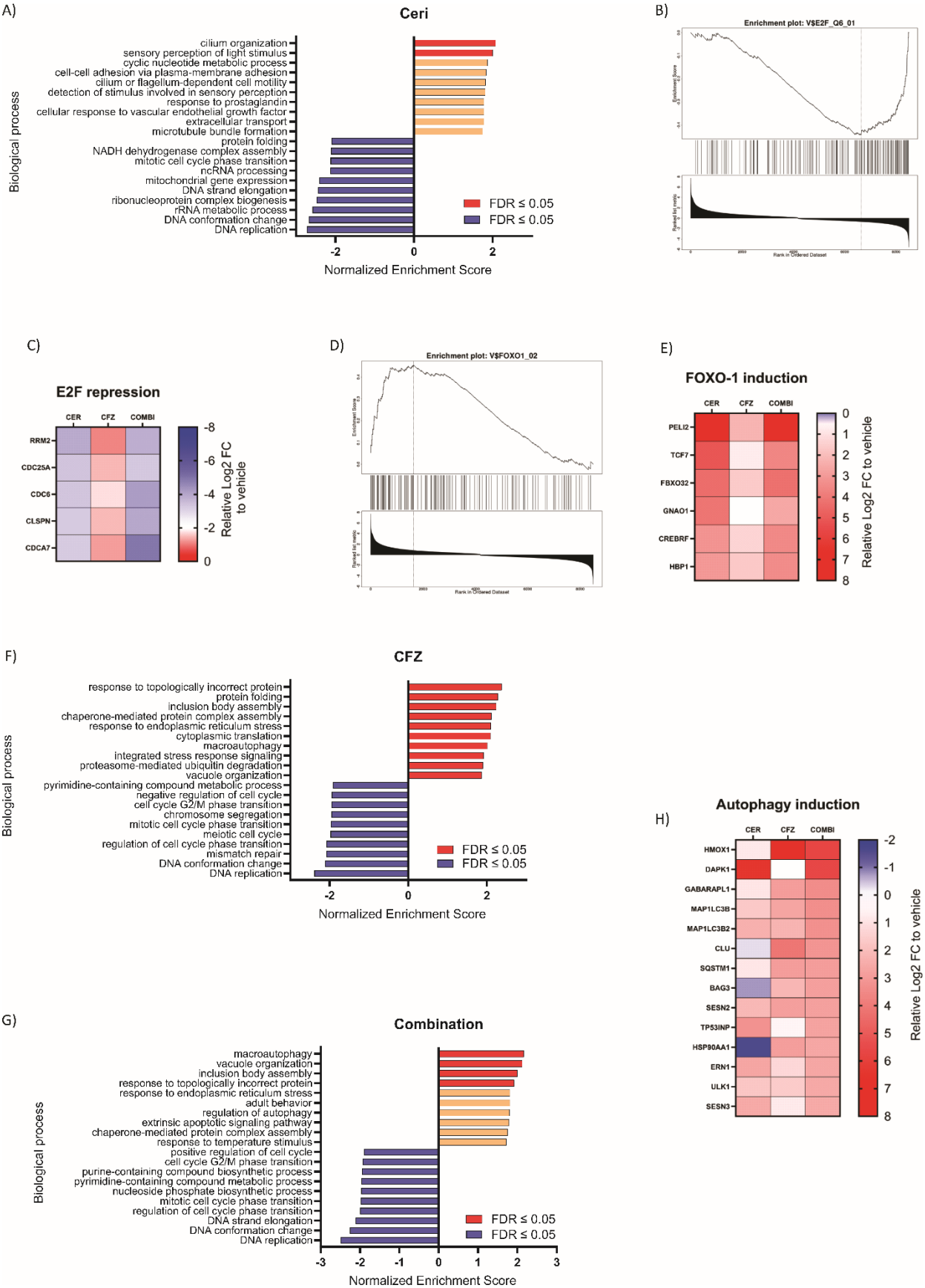

CER: ceritinib; CFZ: carfilzomib; COMBI: combination of ceritinib and carfilzomib; E2F: E2F transcription factor; FOXO1: Forkhead Box O1; GSEA: Gene Set Enrichment Analysis; Log2 FC: Log2 fold change

Figure S11: Levels of HSPA5 (BiP) and HSP70 in cell lines. Quantification of HSPA5 (GRP78/BiP) and HSP70 following western blot analysis, complementing Figures 4H–I.

(A) Changes in HSP70 and HSPA5 levels in AMO-1 cells at 4 and 8 hours after treatment with 4 µM ceritinib, 5 nM carfilzomib, or their combination (C+C).

(B) Changes in HSP70 and HSPA5 levels in L363, AMO-BTZ, and L363-BTZ cells 8 hours after treatment with 5 nM carfilzomib or the combination with 4 µM ceritinib (C+C).

Data represent mean ± SD of three independent experiments. Statistical significance was determined by one-way ANOVA with Tukey's multiple comparisons test: *p < 0.05, **p < 0.01, ***p < 0.001, ****p < 0.0001.

A)

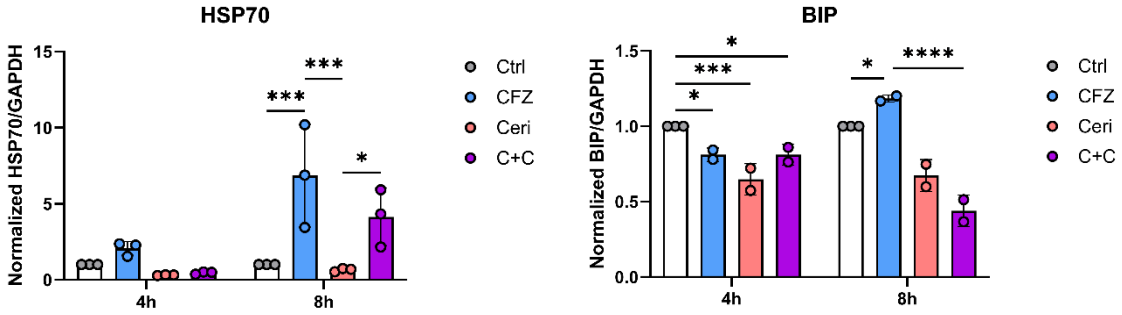

B)

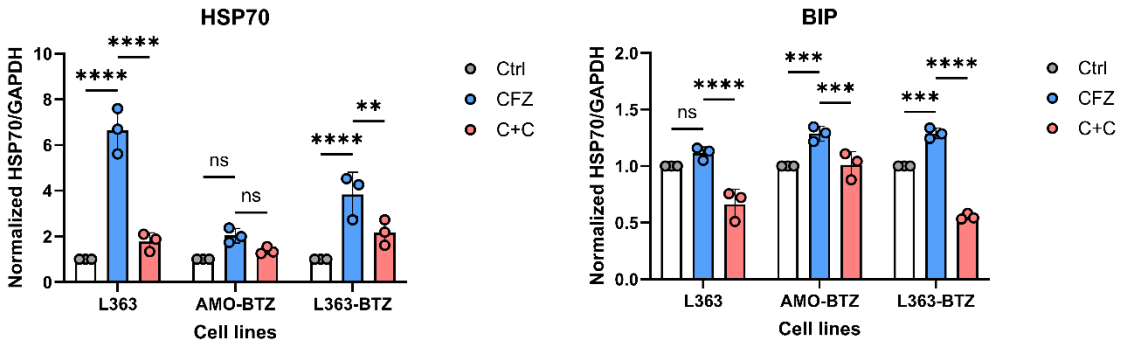

Ceri: ceritinib; CFZ: carfilzomib; GAPDH: Glyceraldehyde-3-Phosphate Dehydrogenase; HSPA5/BiP: Heat Shock 70kDa Protein 5 (Glucose-Regulated Protein, 78kDa)/ Binding-Immunoglobulin Protein; HSP70: Heat Shock 70 KDa Protein.

Figure S12: Levels of PolyUb protein.

Quantification of polyUb following western blot analysis, complementing Figure 5A. Presented are changes in polyUb level in AMO-1 cells at 8 hours after treatment with 4 µM ceritinib, 5 nM carfilzomib, or their combination (C+C). Data represent mean ± SD of three independent experiments. Statistical significance was determined by one-way ANOVA with Tukey's multiple comparisons test: *p < 0.05.

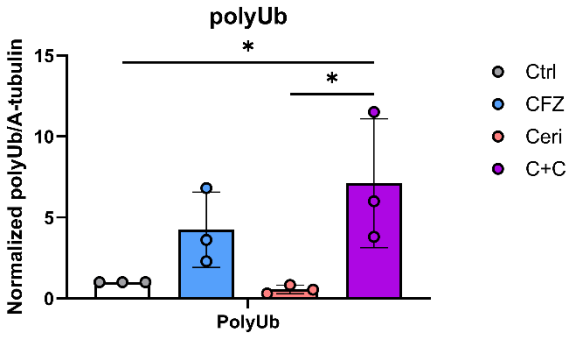

Ceri: ceritinib; CFZ: carfilzomib; polyUb: Ub-K48-linked polyubiquitination

Figure S13: Survival outcomes in newly diagnosed MM patients from the CoMMpass dataset.

Kaplan–Meier survival curves illustrating overall survival of 544 newly diagnosed MM patients stratified by expression levels (high, medium-high, medium-low or low) of **(A)** IGF-1R, **(B)** INSR, **(C)** NPRL3, **(D)** DDIT4, **(E)** FOXO1, **(F)** PDCD4. P value was considered statistically significant at the level $p < 0.05$, statistical significance was assessed by Tarone-Ware test.

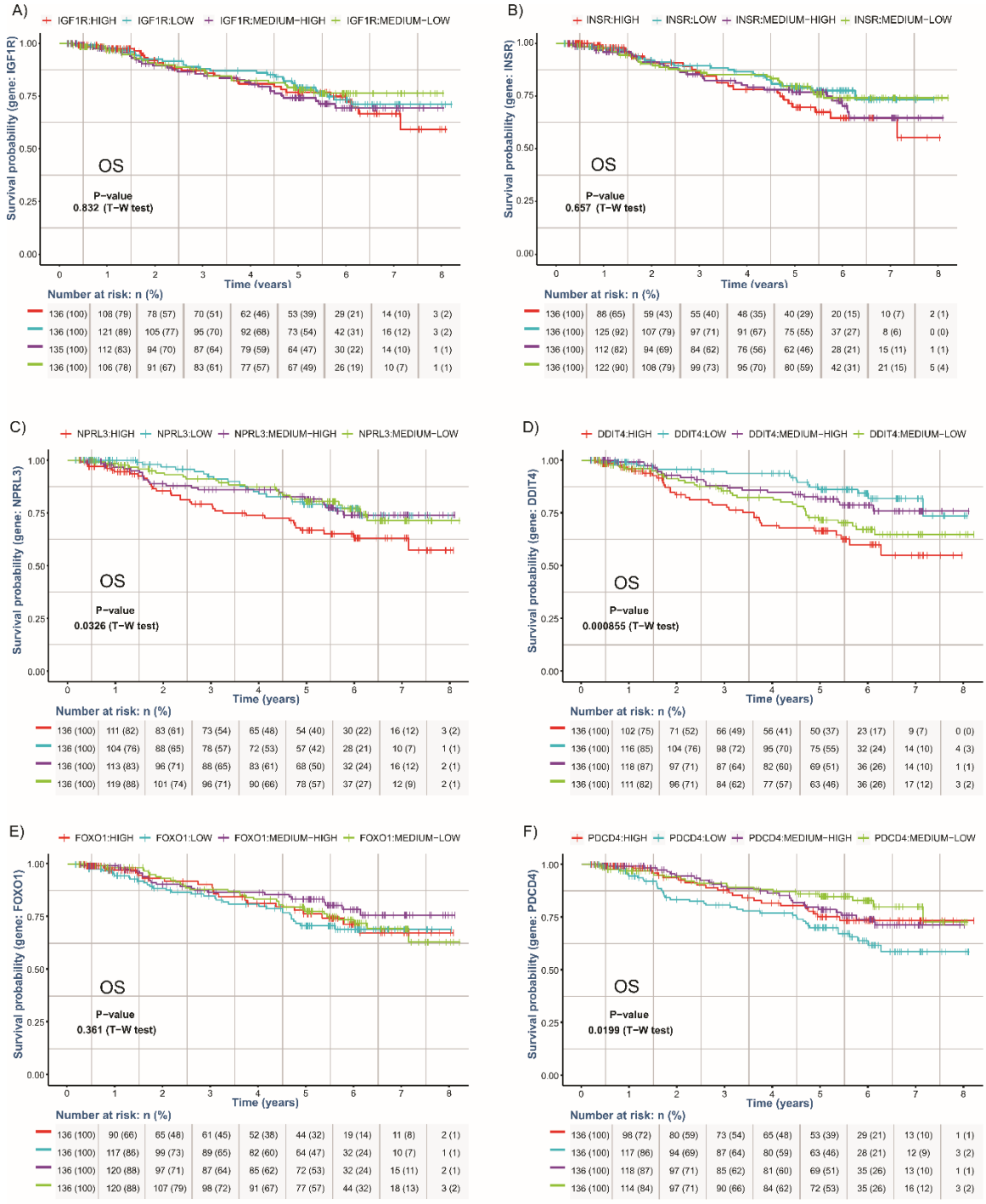

IGF-1R: Insulin Like Growth Factor-1 Receptor; INSR: Insulin Receptor, NPRL3: NPR3 Like, GATOR1 Complex Subunit, DDIT4: DNA Damage Inducible Transcript 4, FOXO1: Forkhead Box O1, PDCD4: Programmed Cell Death 4.

SUPPLEMENTARY TABLES

Supplementary Table S1: Characteristics of MM and PCL samples

	MM PATIENTS		
	MM 35	**MM 42**	**MM 68**
AGE AT SAMPLE COLLECTION	84	74	81
SEX	Male	Female	Female
RELAPSED AFTER	Len, BTZ, CFZ	Len, BTZ, CFZ	Len, BTZ
	PCL PATIENTS		
	PCL 12	**PCL 13**	**PCL 14**
AGE AT SAMPLE COLLECTION	69	51	67
SEX	Female	Female	Female
RELAPSED AFTER	BTZ	Len, Pom, BTZ, CFZ	BTZ, Len

BTZ: Bortezomib; CFZ: Carfilzomib; Len: Lenalidomide; MM: Multiple Myeloma; PCL: Plasma Cell Leukemia; Pom: Pomalidomide

Supplementary Table S2: IC50 values of ALK inhibitors in MM cell lines

Proteasome inhibitor-naïve cell lines (AMO-1 and L363) and bortezomib resistant cell lines (AMO-BTZ and L363-BTZ) were treated with ALK inhibitors for 48h. The IC50 values were determined from the dose-response curves shown in Figure 1A.

	ALK inhibitors IC50 (μM)						
Cell line	**Ceritinib**	**Brigatinib**	**Entrectinib**	**Crizotinib**	**Ensartinib**	**Alectinib**	**Lorlatinib**
L363	1.031	2.472	3.474	3.324	3.7	6.119	21.85
L363-BTZ	0.7891	2.308	4.395	4.151	5.402	6.221	18.53
AMO-1	2.089	1.463	3.511	3.917	4.501	14.13	25.88
AMO-BTZ	2.77	2.667	4.383	6.474	6.252	26.73	37.77

BTZ: bortezomib

Supplementary Table S3: Data from the ChemBL database on the known on-target and off-target activities of various ALK inhibitors.

The drugs are categorized based on their activity in multiple myeloma: the upper section lists ALK inhibitors that are active in MM (Table S1), while the lower section includes those that are less active or inactive. For each drug, the table also specifies the dose required to inhibit the activity of the identified target.

Target (ChEMBL ID)	Actives	Target Name	Brigatinib (nM)		Ceritinib (nM)		Crizotinib (nM)		Entrectinib (nM)	
CHEMBL4247	6	ALK	Active	1	Active	17	Active	103	Active	12
CHEMBL3982	5	FER	Unknown	x	Active	214	Active	269	Active	5
CHEMBL5568	5	ROS	Active	2	Active	9	Active	18	Active	6
CHEMBL1957	4	**IGF-1R**	Active	25	Active	395	Active	335	Active	152
CHEMBL1974	4	**FLT3**	Active	2	Active	516	Active	761	Active	226
CHEMBL1981	4	**INSR**	Active	195	Active	135	Active	527	Active	209
CHEMBL2041	4	RET	Unknown	x	Active	955	Active	1641	Active	124

Target (ChEMBL ID)	Actives	Target Name	Alectinib (nM)		Ensartinib (nM)	Lorlatinib (nM)	
CHEMBL4247	6	ALK	Active	3	Unknown	Active	3
CHEMBL3982	5	FER	Active	3802	Unknown	Active	3
CHEMBL5568	5	ROS	Unknown	x	Unknown	Active	1
CHEMBL1957	4	**IGF-1R**	Inactive	30000	Unknown	Unknown	x
CHEMBL1974	4	**FLT3**	Inactive	30000	Unknown	Unknown	x
CHEMBL1981	4	**INSR**	Inactive	30000	Unknown	Unknown	x
CHEMBL2041	4	RET	Active	41	Unknown	Unknown	x

ALK: Anaplastic Lymphoma Kinase; FER: Feline Encephalitis Virus-Related Kinase; ROS: ROS Proto-Oncogene 1, Receptor Tyrosine Kinase; IGF-1R: Insulin Like Growth Factor 1 Receptor, FLT3: Fms Related Receptor Tyrosine Kinase 3; INSR: Insulin receptor; RET: Ret Proto-Oncogene, Receptor Tyrosine Kinase

Supplementary Table S4: List of ceritinib sensitivity and resistance candidate genes

This table lists the ceritinib sensitivity and resistance candidate genes identified from the genome-wide CRISPR-Cas9 knockout library screen in AMO-1 cells. The genes are ranked based on their false discovery rate (FDR < 0.01) and their overall ranking determined by MAGeCK-VISPR analysis.

Candidate sensitivity genes				
Gene ID	**number of gRNA**	**FDR (negative)**	**Rank (negative)**	**Log2 FC**
PELO	4	0.002475	1	-1.1182
NDUFA6	4	0.002475	2	-1.2656
Candidate resistance genes				
Gene ID	**number of gRNA**	**FDR (positive)**	**Rank (positive)**	**Log2 FC**
FOXO1	4	0.000495	1	2.6339
ZFP36L2	4	0.000495	2	1.6974
FOXO3	4	0.000495	3	1.6506
DDIT4	4	0.000495	4	1.1467
ID3	4	0.000495	5	1.2037
KICS2	4	0.000495	6	2.0332
NPRL3	4	0.000495	7	2.645
NPRL2	4	0.000495	8	1.7576
FAM122A	4	0.000495	9	1.2447
XPNPEP1	4	0.000495	10	1.4268
EIF2AK3	4	0.001142	12	1.3858
RUNX2	4	0.001142	13	1.7436
FIBP	4	0.00165	14	1.4161
SQLE	4	0.00165	15	1.5256
PTEN	4	0.004368	17	1.266
TSC1	4	0.005226	18	1.7607
TSC2	4	0.006514	19	1.0931

PELO, Pelota MRNA Surveillance And Ribosome Rescue Factor; NDUFA6, NADH:Ubiquinone Oxidoreductase Subunit A6; FOXO1, Forkhead Box O1; ZFP36L2, ZFP36 Ring Finger Protein Like 2; FOXO3, Forkhead Box O3; DDIT4, DNA Damage Inducible Transcript 4; ID3, Inhibitor Of DNA Binding 3; KICS2, KICSTOR Subunit 2; NPRL3, NPR3 Like, GATOR1 Complex Subunit; NPRL2, NPR2 Like, GATOR1 Complex Subunit; FAM122A = PABIR1, PP2A Aalpha (PPP2R1A) And B55A (PPP2R2A) Interacting Phosphatase; XPNPEP1, X-Prolyl Aminopeptidase 1; EIF2AK3 = PERK, Eukaryotic Translation Initiation Factor 2 Alpha Kinase 3; RUNX2, RUNX Family Transcription Factor 2; FIBP, FGF1 Intracellular Binding Protein; SQLE, Squalene Epoxidase; PTEN, Phosphatase And Tensin Homolog; TSC1, TSC Complex Subunit 1; TSC2, TSC Complex Subunit 2.

FDR, false discovery rate

Supplementary Table S5: Gene expression and CRISPR-Cas9 dependency scores for BTK, SRC, IGF-1R and INSR

Gene expression and CRISPR-Cas9 dependency scores from the DepMap (DepMap Public 24Q2) for selected cell lines. Each pair of columns represents the CRISPR dependency score and expression level (RNA-seq TPM) for an individual gene across the listed cell lines. Lower CRISPR scores indicate higher gene dependency (essentiality). Expression values are $\log_2$(TPM + 1) normalized. DepMap IDs and corresponding cell line names are provided for reference.

		BTK		SRC		IGF-1R		INSR	
DepMap ID	**Cell Line**	**CRISPR**	**Expression**	**CRISPR**	**Expression**	**CRISPR**	**Expression**	**CRISPR**	**Expression**
ACH-001539	KML1	-0.121	6.921	-0.129	1.556	-0.184	0.189	0.144	0.029
ACH-000889	KMM1	0.139	0.669	-0.138	0.299	-0.754	4.218	-0.227	2.748
ACH-002214	BC1	-0.016	0.098	-0.061	0.189	-0.176	2.436	-0.080	1.623
ACH-002478	BC2	-0.160	0.138	-0.149	0.176	-0.042	1.736	-0.172	0.029
ACH-000024	OPM2	0.095	0.098	-0.130	0.506	-0.484	2.705	-0.134	5.153
ACH-001677	U2904	-0.301	6.360	-0.111	0.333	0.047	2.390	-0.212	2.245
ACH-000363	SKMM2	-0.004	2.087	-0.075	0.151	-0.771	2.094	-0.400	5.250
ACH-000124	OCILY19	-0.108	6.137	-0.164	1.757	-0.687	3.536	-0.243	3.900
ACH-002678	WILL1	-0.233	7.660	-0.354	0.070	-0.522	2.014	-0.155	4.164
ACH-002677	U2946	-0.763	6.245	-0.319	0.029	-0.203	1.157	-0.246	3.058
ACH-000183	L363	0.324	2.325	-0.201	0.390	-0.799	3.445	-0.210	4.129
ACH-000167	KE97	0.016	6.121	-0.242	4.852	-0.007	1.722	-0.055	3.274
ACH-000763	MM1S	0.150	3.014	-0.198	2.087	-0.913	2.870	-0.543	3.285
ACH-000714	KMS11	0.021	0.163	-0.140	0.239	-0.980	4.275	-0.356	3.698
ACH-000838	AMO1	-0.173	4.216	-0.052	0.799	-1.164	2.325	-0.516	3.992
ACH-000829	HUNS1	-0.026	6.292	-0.100	4.320	-0.114	0.029	0.021	3.540
ACH-000821	EJM	0.025	6.017	-0.220	0.275	-0.213	2.138	-0.153	4.139
ACH-000817	RPMI8226	0.104	3.909	-0.016	0.575	-0.543	2.850	-0.152	2.425
ACH-000512	INA6	-0.183	6.624	0.005	5.304	-0.612	2.444	-0.207	4.496
ACH-000541	KMS34	0.234	0.444	-0.118	0.322	-0.365	3.051	0.046	4.548
ACH-000653	JJN3	0.015	1.124	-0.134	1.202	-0.588	3.053	-0.266	3.457
ACH-000576	KMS27	0.088	3.352	-0.021	0.895	-0.596	1.986	-0.193	3.048
ACH-000588	KMS26	0.007	1.718	0.026	0.275	-0.511	4.055	-0.344	3.904

Supplementary Table S6: Differentially expressed genes identified by NGS

A list of the differentially expressed genes between control cells and cells treated with ceritinib, carfilzomib, or the drug combination. Data is provided in a separate Excel sheet.

Supplementary Table S7: Top 10 positive and top 10 negative enriched biological process categories deregulated by ceritinib treatment

A list of the top 10 positively and top 10 negatively enriched biological process categories, as determined by Gene Ontology (GO) analysis. The categories were derived from Gene Set Enrichment Analysis (GSEA) of differentially expressed genes between ceritinib-treated and control cells. Significantly deregulated processes are highlighted in bold (positive in light red, negative in light blue).

Gene Set	Description	Size	Leading Edge Number	NES	FDR
GO:0044782	cilium organization	232	110	2.0769	0.022359
GO:0050953	sensory perception of light stimulus	54	28	1.9992	0.031542
GO:0009187	cyclic nucleotide metabolic process	15	7	1.8727	0.11312
GO:0098742	cell-cell adhesion via plasma-membrane adhesion molecules	60	19	1.8372	0.13056
GO:0001539	cilium or flagellum-dependent cell motility	48	29	1.8203	0.12824
GO:0050906	detection of stimulus involved in sensory perception	22	12	1.8152	0.11286
GO:0034694	response to prostaglandin	10	4	1.7802	0.14818
GO:0035924	cellular response to vascular endothelial growth factor stimulus	31	10	1.7786	0.13156
GO:0006858	extracellular transport	19	15	1.7777	0.11809
GO:0001578	microtubule bundle formation	45	24	1.748	0.14789
GO:0006457	protein folding	143	67	-2.0946	0.0057124
GO:0010257	NADH dehydrogenase complex assembly	45	37	-2.1062	0.0056961
GO:0044772	mitotic cell cycle phase transition	288	77	-2.1241	0.0051265
GO:0034470	ncRNA processing	311	156	-2.1325	0.0052311
GO:0140053	mitochondrial gene expression	137	100	-2.4146	2.20E-16
GO:0022616	DNA strand elongation	32	20	-2.4453	2.20E-16
GO:0022613	ribonucleoprotein complex biogenesis	350	241	-2.4779	2.20E-16
GO:0016072	rRNA metabolic process	196	117	-2.5847	2.20E-16
GO:0071103	DNA conformation change	72	36	-2.6748	2.20E-16
GO:0006260	DNA replication	208	98	-2.7215	2.20E-16

GeneSet: ID of the gene set; **Description:** Name/Description of the gene set; **Size:** Number if genes in the set after filtering; **Leading Edge Number:** Number of genes in the leading edge; **NES:** Normalized Enrichment Score, enrichment score normalized to average enrichment score of all permutations; **FDR:** p value corrected for multiple testing

Supplementary Table S8: Top 10 positive and top 10 negative enriched biological process categories deregulated by carfilzomib treatment

A list of the top 10 positively and top 10 negatively enriched biological process categories, as determined by Gene Ontology (GO) analysis. The categories were derived from Gene Set Enrichment Analysis (GSEA) of differentially expressed genes between carfilzomib-treated and control cells. Significantly deregulated processes are highlighted in bold (positive in light red, negative in light blue).

Gene Set	Description	Size	Leading Edge Number	NES	FDR
GO:0035966	response to topologically incorrect protein	112	31	2.3745	2.20E-16
GO:0006457	protein folding	143	45	2.2825	4.90E-04
GO:0070841	inclusion body assembly	17	8	2.2393	6.54E-04
GO:0051131	chaperone-mediated protein complex assembly	18	7	2.1186	1.72E-03
GO:0034976	response to endoplasmic reticulum stress	179	44	2.0997	1.77E-03
GO:0002181	cytoplasmic translation	106	64	2.094	1.47E-03
GO:0016236	macroautophagy	227	62	2.0113	0.0046237
GO:0140467	integrated stress response signaling	34	8	1.92	0.020106
GO:0043161	proteasome-mediated ubiquitin-dependent protein catabolic process	306	105	1.901	0.023103
GO:0007033	vacuole organization	154	42	1.8661	0.029334
GO:0072527	pyrimidine-containing compound metabolic process	48	21	-1.9225	0.0068098
GO:0045786	negative regulation of cell cycle	239	82	-1.9448	0.0056466
GO:0044839	cell cycle G2/M phase transition	104	34	-1.9475	0.0059713
GO:0007059	chromosome segregation	287	108	-1.9583	0.0047915
GO:0044772	mitotic cell cycle phase transition	288	93	-1.9629	0.0052513
GO:0051321	meiotic cell cycle	132	51	-1.9774	0.0056918
GO:1901987	regulation of cell cycle phase transition	283	97	-2.0795	0.00076229
GO:0006298	mismatch repair	22	12	-2.0809	0.0010164
GO:0071103	DNA conformation change	72	32	-2.1136	0.00050819
GO:0006260	DNA replication	208	89	-2.3881	2.20E-16

GeneSet: ID of the gene set; **Description:** Name/Description of the gene set; **Size:** Number if genes in the set after filtering; **Leading Edge Number:** Number of genes in the leading edge; **NES:** Normalized Enrichment Score, enrichment score normalized to average enrichment score of all permutations; **FDR:** p value corrected for multiple testing.

Supplementary Table S9: Top 10 positive and top 10 negative enriched biological process categories deregulated by combination treatment

A list of the top 10 positively and top 10 negatively enriched biological process categories, as determined by Gene Ontology (GO) analysis. The categories were derived from Gene Set Enrichment Analysis (GSEA) of differentially expressed genes between combination-treated and control cells. Significantly deregulated processes are highlighted in bold (negative in light blue, positive in light red).

Gene Set	Description	Size	Leading Edge Number	NES	FDR
GO:0016236	macroautophagy	227	94	2.1637	2.83E-03
GO:0007033	vacuole organization	154	65	2.1237	0.0047086
GO:0070841	inclusion body assembly	17	7	2	0.015695
GO:0035966	response to topologically incorrect protein	112	32	1.915	0.038846
GO:0034976	response to endoplasmic reticulum stress	179	45	1.815	0.10284
GO:0030534	adult behavior	49	21	1.8136	0.087266
GO:0010506	regulation of autophagy	234	87	1.8016	0.083679
GO:0097191	extrinsic apoptotic signaling pathway	125	33	1.7927	0.082518
GO:0051131	chaperone-mediated protein complex assembly	18	6	1.7563	0.10704
GO:0009266	response to temperature stimulus	92	24	1.7186	0.13796
GO:0045787	positive regulation of cell cycle	180	58	-1.8999	0.011061
GO:0044839	cell cycle G2/M phase transition	104	42	-1.9322	0.010624
GO:0072522	purine-containing compound biosynthetic process	159	100	-1.9539	0.0081846
GO:0072527	pyrimidine-containing compound metabolic process	48	22	-1.9629	0.0075721
GO:1901293	nucleoside phosphate biosynthetic process	181	110	-1.9724	7.62E-03
GO:0044772	mitotic cell cycle phase transition	288	106	-1.9793	7.90E-03
GO:1901987	regulation of cell cycle phase transition	283	105	-2.0056	6.24E-03
GO:0022616	DNA strand elongation	32	19	-2.1177	2.20E-16
GO:0071103	DNA conformation change	72	29	-2.2566	2.20E-16
GO:0006260	DNA replication	208	98	-2.4918	2.20E-16

GeneSet: ID of the gene set; **Description:** Name/Description of the gene set; **Size:** Number if genes in the set after filtering; **Leading Edge Number:** Number of genes in the leading edge; **NES:** Normalized Enrichment Score, enrichment score normalized to average enrichment score of all permutations; **FDR:** p value corrected for multiple testing.

Supplementary Table S10: List of identified metabolites and their differential expression. (Separate excel file).

Column Headings:

Metabolite ID: Ion ID, consisting of RT and m/z, ie "RT_m/z" (retention time_mass-to-charge ratio).

Fold change: Fold change (variation multiple), according to the group ratio in the file name.

Log2 FC: Log2 of fold change.

Change: change in the treatment condition vs the control.

P value: The test and statistical significance used to screen for differential ions.

Q value: The test and statistical significance used to screen for differential ions corrected for multiple testing.

VIP: Variable important for the projection, indicating the contribution of m/z to the PLSDA model.

Sample: Comparison group.

Ion Mode:

RT: retention time, (in min), indicates the time in the liquid chromatograph when the maximum concentration of the component appears after sample entering LC for separation.

Molecular Weight: Metabolite molecular weight

Formula: Metabolite chemical formula

Name: Substance Name

Database: Classification according to KEGG or HMDB

KEGG ID: Kyoto Encyclopedia of Genes and Genomes (KEGG) database number.

HMDB ID: Human Metabolome Database (HMDB) database number.

Super class: Substance classification information.

Sub Class: Second-level classification information.

Class: Third-level classification information.

Super Pathway: Substance classification information based on the metabolic pathways

Sub Pathway: Second-level classification information based on the metabolic pathways

Pathway: Third-level classification information based on the metabolic pathways

State: Significant or non-significant classification, based on the p value

SUPPLEMENTARY REFERENCES

1. Chen L, Ye HL, Zhang G et al. Autophagy inhibition contributes to the synergistic interaction between EGCG and doxorubicin to kill the hepatoma Hep3B cells. *PLoS One*. 2014; 9(1):e85771.

2. de Bruin G, Xin BT, Kraus M et al. A Set of Activity-Based Probes to Visualize Human (Immuno)proteasome Activities. *Angew Chem Int Ed Engl*. 2016; 55(13):4199-203.

3. Ferguson ID, Patino-Escobar B, Tuomivaara ST et al. The surfaceome of multiple myeloma cells suggests potential immunotherapeutic strategies and protein markers of drug resistance. *Nat Commun*. 2022;13(1):4121.

4. Love MI, Huber W, Anders S. Moderated estimation of fold change and dispersion for RNA-seq data with DESeq2. *Genome Biol*. 2014;15(12):550.

5. Kaplan EL, Meier P. Nonparametric Estimation from Incomplete Observations. *Journal of the American Statistical Association*. 1958 1958/06/01;53(282):457-481.

6. Tarone RE, Ware J. On distribution-free tests for equality of survival distributions. *Biometrika*. 1977;64(1):156-160.

7. Wickham H, Hester J, Bryan J. readr: Read Rectangular Text Data. R package version 2.1.5; 2024.

8. Wickham H. stringr: Simple, Consistent Wrappers for Common String Operations. R package version 1.5.1; 2023.

9. Wickham H. ggplot2: Elegant Graphics for Data Analysis. Springer-Verlag New York; 2016.

10. Therneau TM, Grambsch PM. Modeling Survival Data: Extending the Cox Model. New York: Springer Science+Business Media; 2000.

11. Wickham H, Averick M, Bryan J et al. Welcome to the Tidyverse. *Journal of Open Source Software*. 2019;4(43):1686.

12. Dragulescu A, Arendt C. xlsx: Read, Write, Format Excel 2007 and Excel 97/2000/XP/2003 Files. 2020. R package.

13. Wu T, Hu E, Xu S et al. clusterProfiler 4.0: A universal enrichment tool for interpreting omics data. *Innovation (Camb)*. 2021;2(3):100141

14. Kassambara A, Kosinski M, Biecek P. survminer: Drawing Survival Curves using 'ggplot2'. 2024.

15. Hothorn T, Hornik K, van de Wiel MA, Zeileis A. A Lego System for Conditional Inference. The American Statistician. 2006; 60(3):257-263.

16. Robinson MD, McCarthy DJ, Smyth GK. edgeR: a Bioconductor package for differential expression analysis of digital gene expression data. Bioinformatics. 2010; 26(1):139-140.

17. Munawar U, Zhou X, Prommersberger S et al. Impaired FADD/BID signaling mediates cross-resistance to immunotherapy in Multiple Myeloma. *Commun Biol*. 2023; 6(1):1299.

18. Rajkumar SV, Harousseau JL, Durie B et al. Consensus recommendations for the uniform reporting of clinical trials: report of the International Myeloma Workshop Consensus Panel 1. *Blood*. 2011; 117(18):4691-4695.

19. Wen B, Mei Z, Zeng C, Liu S. metaX: a flexible and comprehensive software for processing metabolomics data. *BMC Bioinformatics*. 2017; 18(1):183.

20. Pang Z, Zhou G, Ewald J et al. Using MetaboAnalyst 5.0 for LC-HRMS spectra processing, multi-omics integration and covariate adjustment of global metabolomics data. *Nat Protoc*. 2022; 17(8):1735-1761.

21. Tanida I, Ueno T, Uchiyama Y. A super-ecliptic, pHluorin-mKate2, tandem fluorescent protein-tagged human LC3 for the monitoring of mammalian autophagy. *PLoS One*. 2014; 9(10):e110600.

22. Nougarede A, Tesniere C, Ylanko J, Rimokh R, Gillet G, Andrews DW. Improved IRE1 and PERK Pathway Sensors for Multiplex Endoplasmic Reticulum Stress Assay Reveal Stress Response to Nuclear Dyes Used for Image Segmentation. *Assay Drug Dev Technol*. 2018; 16(6):350-360.

23. Besse A, Besse L, Kraus M et al. Proteasome Inhibition in Multiple Myeloma: Head-to-Head Comparison of Currently Available Proteasome Inhibitors. *Cell Chem Biol*. 2019; 26(3):340-351.e3.

24. Gross SM, Rotwein P. Akt signaling dynamics in individual cells. *J Cell Sci*. 2015; 128(14):2509-2519.

25. Hay N. Interplay between FOXO, TOR, and Akt. Biochim Biophys Acta. 2011; 1813(11):1965-1970.